BIO-POLYMERIC MATERIALS FOR ELECTRICAL INSULATION APPLICATIONS

by

LAKSHAN WARNAKULASOORIYA

A thesis submitted to the Faculty of Graduate Studies of
The University of Manitoba
in partial fulfillment of the requirements for the degree of

MASTER OF SCIENCE

Department of Electrical and Computer Engineering
University of Manitoba
Winnipeg, Manitoba, Canada

Abstract

Fossil-fuel-based insulation materials such as polyvinyl chloride (PVC), low-density polyethylene (LDPE), cross-linked polyethylene (XLPE) and ethylene-vinyl acetate (EVA) have dominated the electrical insulation industry at present. Increased use of these polymers have caused a serious threat to environment causing, environmental pollution, global warming, and climate changes worldwide. Biopolymers offers a solution to these problems, since they are fully renewable from bio-sources such as biomass, agricultural by-products, and biological waste. In order to utilize biopolymers as an electrical insulation material, they should match or exceed electrical, mechanical, and thermal properties of their fossil-fuel-based counterparts. Four bio-polymers namely polyhydroxy butyrate (PHB), poly(3-hydroxybutyrate-co-3-hydroxyvalerate) (PHBV), poly (lactic acid) (PLA), cellulose acetate (CA) and three fossil-fuel-based synthetic polymers polycaprolactone (PCL), polybutylene succinate (PBS), poly (butylene adipate-co-terephthalate) (PBAT) are selected based on their popularity in research and commercial availability. Although commercial manufacturing of these four synthetic polymers is from fossil-fuel-based sources, they can be synthesised from bio-sources as well. Samples of six of these selected polymers, PHB, PHBV, PCL, PBS, and PBAT are obtained collaborating with the Biosystems Engineering department for the electrical measurements. These samples are thin films, prepared from spin-casting process. Electrical properties such as complex dielectric constant, volume resistivity and AC electrical breakdown strength of these samples are measured, while thermal and mechanical properties are summarized from literature. Using experimental measurements and the literature data, properties of these selected polymers are compared with conventional polymers such as PVC, LDPE, XLPE and EVA. Few biopolymers are shortlisted as possible candidate materials for electrical insulation applications.

Acknowledgements

First and foremost, I would like to express my sincere gratitude to my advisor Prof. Derek Oliver for his support and guidance throughout my research. He was always there for support, guidance, motivation, and encouragement throughout every step of my masters. He has definitely been more than just an academic advisor, it was a privilege to work under his supervision. I also would like to thank Professor Behzad Kordi for supporting me on lab experiments. His experience in high voltage electrical insulation material testing helped me to carryout the lab experiments in confidence.

I would like to thank my examining committee, for accepting to review this thesis and providing constructive comments.

I convey my sincere appreciation to my colleagues at the Electrical and Computer Engineering department (ECE), for their support and allowing me to take the time necessary to complete the lab work. Also, I would like to thank Quintin Litke from the department of Biosystems Engineering who manufactured the polymer samples for electrical measurements.

Last but not least, I would like to thank my family for their continuous support and encouragement. A special and profound thanks goes out to my spouse Sachithra Opathalage, who's support was unconditional, and was there for me and aided me through this process.

Dedication

To my loving family.

TABLE OF CONTENTS

Chapter 1

Introduction

1.1 History of electrical insulation materials

The technological development of electrical systems was the driving force behind the advancement of electrical insulation materials. The idea of electrical insulation began with the inception of early electrical systems. Naturally-occurring materials such as rubber, mica, oil-impregnated paper, cotton thread, and fabric were some of the insulation materials used in earlier electrical systems [1]. But these materials had drawbacks such as poor durability, complex installation methods, higher cost and most of all high rates of insulation failures. This lead towards using fossil-fuel-based polymers as electrical insulators. Polyethylene (PE) and polyvinyl chloride (PVC) were the first fossil-fuel-based polymers to be used in electrical systems. However, when first introduced, PE and PVC had many drawbacks [2]. PE had a low softening temperature which made it unsuitable for applications beyond 70 °C. Earlier PVC compounds had high electrical losses and could only withstand low voltages upto 1000 V [1]. These issues were solved later when scientists developed cross-linking reactions to generate cross linked polyethylene (XLPE), which was capable of with-

standing higher voltages. Earlier XLPE cables could withstand voltages up to 230 kV [1], whereas at present XLPE cables could reach up to 500 kV [3], [4]. Also, development of plasticizers and additives made PVC cables more flexible, durable, and heat resistant [3]. More and more low-voltage PVC cable products emerged in the global wires and cables market due to low cost, fully synthetic production, ease of extrusion and vulcanization free production process. On the other hand, XLPE cables dominated the medium voltage and high voltage electrical cable market due to low cost, reliability, and superior dielectric strength. Eventually, the electrical wires and cables industry has completely shifted towards using fossil-fuel-based electrical insulation materials.

1.2 Problem Description

Today, the power cable industry relies on fossil-fuel-based polymeric insulators. Materials such as polyvinyl chloride (PVC), ethylene-vinyl acetate (EVA), cross-linked polyethylene (XLPE) have become industrial norms when it comes to polymeric insulators [5]. Fossil-fuel-based polymeric insulation systems have evolved through decades of research and development. However, fossil fuel is a non-renewable resource. With the current consumption rate it is said the worldwide fossil fuel reserves will be completely exhausted by year 2100 [6]. The use of fossil fuels has increased carbon emissions causing global warming and climate changes worldwide. Additionally, there is an increasing concern for environmental pollution caused by non-biodegradable plastics generated as a byproduct of fossil-fuel production. Small fractions of these plastic products are recycled whereas, most end-up in a landfill or in the ocean. Ocean litter is embedded into marine life and make way into the food chain, while methane gas is released from landfills [7]. Due to these pressing issues

there is a drive towards renewable energy and renewable resources. Bio-based materials can be fully renewable when generated from bio-based sources such as corn-starch, sugarcane and ethanol byproducts or microbial digestion processes. These bio-based materials can provide solutions to many of the problems caused by fossil-fuel-based materials. With these intentions in mind more and more bio-based materials are emerging into the consumer market and bio-based electrical insulation systems are gaining much interest recently. To replace conventional fossil-fuel-based polymeric insulation materials, bio-based materials should outperform or match their electrical, mechanical and thermal properties. Therefore, a comprehensive investigation of these properties is necessary to identify suitable candidate materials for complete replacement or further development.

1.3 Objective of the thesis

The objective of this thesis is to explore the feasibility of replacing fossil-fuel-based conventional polymeric insulation materials with bio-based polymeric insulation materials. To do this, one should benchmark their properties with known polymeric insulation materials. As discussed earlier, LDPE, XLPE, PVC, EVA and Nylon 6 are commonly used in electrical power cables [5]. However, the literature review indicates that many important electrical properties of bio-based polymers are yet to be explored. Specifically, dielectric and electric breakdown properties of bio-based polymers are unavailable. These properties are essential to benchmark them among conventional fossil fuel based polymers. Hence, in this thesis the focus is mainly on investigating these missing properties and comparing them with available literature data. With our experimental values and literature values we then move onto critically analysing possible candidates for future polymeric insulation systems.

1.4 Contributions

This thesis provides a conscious summery of existing research on bio-polymeric insulation materials and their electrical,mechanical and thermal properties. AC breakdown strength, complex dielectric constant and volume resistivity is experimentally measured, whereas AC breakdown strength of PHB, PHBV and PBAT is measured for the first time in research history. Also, by-far this is the only study that reports AC breakdown strength measurements of PHB, PHBV, PCL, PBS, PBAT and PLA following ASTM D149 standard [8]. Furthermore, complex dielectric constant and volume resistivity are measured for PHB, PHBV, PCL, PBS, PBAT and PLA using a similar test setting, allowing them to be compared with each other. Using the experimental findings and literature data, performance of bio-polymers are compared with conventional polymers to identify suitable candidate materials for electrical insulation applications.

1.5 Organization of Thesis

In Chapter 2, a review of research done on bio-based electrical insulation materials available in the literature is presented. A few bio-based electrical insulation materials were selected along with their fossil-fuel-based counterparts for comparison. This selection was based on the popularity in research literature and commercial availability. Next we discussed their electrical, mechanical and thermal properties and summarize the values reported in research literature. From our investigation, we found that some electrical properties of bio-based polymers are yet to be explored. Electrical tests on these materials were done to obtain these missing information, which was described in the following chapter.

Samples of polyhydroxybutyrate (PHB), poly(3-hydroxybutyrate-co-3-hydroxyvalerate) (PHBV), polycaprolactone (PCL), polybutylene succinate (PBS), poly(butyleneadipate-co-terephthalate) (PBAT) and poly(lactic acid) (PLA) were obtained from our collaborator at the Department of Biosystems Engineering. It should be noted that, PHA, PHBV, and PLA are bio-polymers derived from renewable source, whereas PCL, PBS, and PBAT are biodegradable polyesters derived from fossil-fuels. Next, we describe the sample preparation methodology and origin of the raw materials used by the collaborator in Chapter 3. Then, measurements of dielectric properties including, dielectric breakdown strength, complex relative permittivity and volume resistivity is described. We focused our study on the measurement of electrical properties, whereas thermal and mechanical properties were summarized from recent literature in the previous chapter. In Chapter 4, we compare the experimental results with the values reported in the literature. Electrical, mechanical, and thermal properties of the selected polymers are critically analyzed to identify potential candidate materials for further enhancement. Finally, in Chapter 5 we conclude by summarizing our findings and explaining the possibilities for replacing fossil-fuel-based polymers with bio-based polymers for electrical insulation applications.

Chapter 2

Background and Literature Review

2.1 Materials of Interest

Our interest lies in the use of renewable polymeric materials for electrical insulation applications. These materials can be generated directly from a bio-source such as bacterial digestion or can be synthesised chemically from a bio-source. These bio-sources originates from agriculture, forestry or in many cases can be derived from biological waste. Also, commercially available bio-based materials were selected since our interest in the thesis was bench-marking their properties with existing fossil-fuel-based electrical insulation rather than synthesising new materials. With this criteria in mind polymeric insulation materials were selected from the recent research literature to summarize their electrical, mechanical, and thermal properties. A list of commonly-used polymeric materials is given in Table 2.1. Origin, chemical structure, and more information on these polymers are described in Appendix A.

Table 2.1. *List of polymers considered in this study.*

Abbreviation	Polymer name
PHB	Polyhydroxybutyrate
PHBV	Poly(3-hydroxybutyrate-co-3-hydroxyvalerate)
PCL	Polycaprolactone
PBS	Polybutylene succinate
PBAT	Poly(butylene adipate-co-terephthalate)
PLA	Poly(lactic acid)
CA	Cellulose acetate
LDPE	Low density polyethylene
XLPE	Cross linked polyethylene
PVC	Poly Vinyl chloride
EVA	Ethylene vinyl acetate
NYLON 6	Polycaprolactam

2.2 Trends in bio-polymers.

Bio-polymer materials are emerging in many applications, mainly in food packaging, biomedical implants and also in electrical insulation industry. The concept of using bio-polymers in electrical insulation applications is novel compared to their other applications. Few research groups around the world have researched on the electrical properties of bio-polymers. Mainly researchers in Japan and France have contributed to these investigations.

Japanese researches such as Y. Ohki [9], N. Hirai [10], K.Shinyama [11] and Y. Maeno [12] have researched polymers including PLA, PBS, ϵ-polycaprolactone butylene succinate (PCL-BS), polybutylene succinate adipate (PBSA), PBAT, PCL and PHBV. They have researched mainly on the complex dielectric, dielectric breakdown

strength, conduction current, glass transition and melting temperatures of these polymers. However, the dielectric breakdown strength measurements done by these researches are based on a McKeown-type electrode system, where the samples are prepared by fixing a thin sheet between two spherical electrodes in epoxy resin medium. This methods is not comparable with ASTM D149 standard [8], which is widely used in North America. Researchers such as V. Hegde [13], O. Gallot [14] have contributed from France, whereas their main focus is reviewing properties of bio-polymers and investigating relative permittivity, dissipation factor, apparent conductivity and DC breakdown strength. Their experimental findings are based on PHBV and PCL, whereas properties of PHB, PCL-BS, PBS, PBSA, PBAT, PLA, PETS and CA are summarized from literature. By-far these are the only review studies available in research literature which compare properties of several bio-polymers. There are many other researchers who has researched on an individual polymer or an individual property. Considering up to date research literature, there is no published research on the dielectric breakdown strength of PHB, PCL, PBAT and CA. Understanding the basic properties of bio-polymers is important before developing specific electrical insulation applications such as cables, insulators and coatings. Nevertheless, understanding the theoretical concepts and standards behind these properties and measurements is important if we are to compare the work of multiple researchers. An overview of the electrical, mechanical and thermal properties, as well as measurements reported in literature are summarized for selected polymers in the next few sections.

2.3 Electrical Properties.

2.3.1 Response of dielectrics to electric field

Of the two large classes of materials, most polymers fall under electrical insulators or dielectrics. In dielectrics, charges are attached to individual molecules unlike conductors which have free electrons. When an external electrical field is applied to a dielectric material, a dipole moment is induced causing the material to be polarized. This dipole moment depends on the molecular polymer chains, which can be inherently polar (permanent dipole) or the electric field can induce a slight shift in charge causing a temporary dipole.

Consider a vacuum parallel plate capacitor having a surface area of A and a electrode separation distance of d as shown in figure 2.1. The charge stored in the capacitor (Q_0) is given by,

$$Q_0 = A\epsilon_0 E \tag{2.1}$$

where ϵ_0 is the permittivity of free space which is equal to $8.85 \times 10^{-12} F/m$ and E is the electric field intensity. Now a homogeneous dielectric with a dielectric constant ϵ is inserted between the parallel plates. The charge stored in the new system is given by,

$$Q_1 = A\epsilon_0\epsilon E. \tag{2.2}$$

The increase in the stored charge is,

$$Q_1 - Q_0 = AE\epsilon_0(\epsilon - 1) \tag{2.3}$$

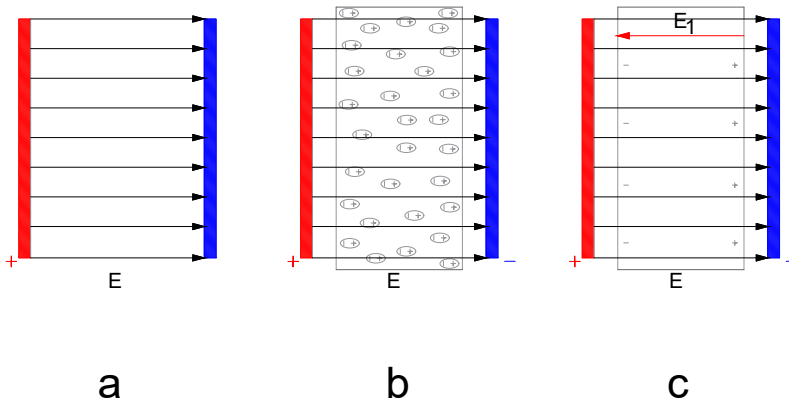

Figure 2.1. *(a) Schematic of a parallel plate capacitor in vacuum, (b) homogeneous dielectric inserted between the plates and dipoles oriented according to the electric filed E_0 (c) resultant electrical field created by dipole orientation E_1*

The dipole moment due to the increase in charge can be given by,

$$\mu = AE\epsilon_0(\epsilon - 1)d. \tag{2.4}$$

Hence, dipole moment per unit volume is

$$P = E\epsilon_0(\epsilon - 1) = \epsilon_0\chi_e E \tag{2.5}$$

where P is also called the polarization and χ_e is the electric susceptibility of the material.

Polarization of the dielectric may occur due to different polarization mechanisms. The total polarization P_t will be the sum of mechanisms such as electronic polarization P_e, atomic polarization P_i, orientational polarization P_d, and the interfacial polarization P_s.

Matter consists of atoms, which in turn, consist of atomic nuclei and a cloud

of electrons. Electronic polarization occur when the applied electrical field displaces the cloud of electrons relative to the atomic nuclei. In the absence of an external electric field, the centroid of the electron cloud coincides with the centroid of the nucleus. Thus, the displacement of the electron cloud results in a dipole moment. When an applied electric field is alternating at a certain frequency, the electron cloud displacement is capable of syncing with the electric field up to frequencies in the range of $10^{14} - 10^{15}$Hz. Above these frequencies electron cloud is not capable of keeping in phase, hence contribution from electronic polarization diminishes.

Atomic polarization occurs when the atomic nuclei is displaced relative to another atom that forms the molecule in presence of an electric field. This polarization mechanism exists when the molecule is made up of dissimilar atoms bonded with polar bonds. Atomic polarization is prominent when these polar bonds are weaker. However, in the presence of an electric field, atomic displacement is superimposed on the displacement of electron cloud discussed earlier. The charge displacement around the nuclei during electronic polarization will change the bond length and bond angle, therefore atomic displacement is connected with electronic polarization. Atomic polarization is common in ionic crystals such as KCl, NaCl etc. Also, polymer chains with different side groups show atomic polarization. Atomic polarization mechanism is dominant in the frequency range of $10^{11} - 10^{14}$Hz.

Some molecules are formed of dissimilar elements and are not symmetrical. These molecules show a permanent dipole moment. For example, the water molecule H_2O behaves as a permanent dipole due to its asymmetrical chemical structure. In the presence of an electrical field, the orientation of the molecules can change creating a orientational polarization. This polarization mechanism is effective in the range of $10^6 - 10^9$Hz.

Interfacial polarization is different from the other polarization mechanisms dis-

cussed earlier. Interfacial or space charge polarization occur when charges drift through the material and accumulate at interfaces. This charge buildup can occur in the volume or on the surface due to the change in conductivity at boundaries such as cracks, imperfections and boundaries between crystalline and amorphous regions. The effect of interfacial polarization on the real, $\epsilon^{'}$, and imaginary, $\epsilon^{''}$ parts of the complex permittivity has been derived by Maxwell-Wagner [15]. Consider a two layer dielectric with dielectric constants ϵ_1 and ϵ_2 and resistivity ρ_1 and ρ_2 as illustrated in Figure 2.2. When a voltage V is applied to the dielectric at $t = 0$ the voltage across

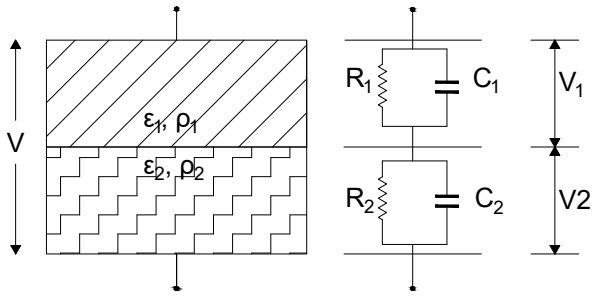

Figure 2.2. *Two layer polymer and the series equivalent circuit representation.*

each layer is distributed as,

$$V_{1,t=0} = V\frac{C_2}{C_1 + C_2} \tag{2.6}$$

$$V_{2,t=0} = V\frac{C_1}{C_1 + C_2}. \tag{2.7}$$

At steady state $t \to \infty$ the voltages will be,

$$V_{1,t\to\infty} = V\frac{R_1}{R_1 + R_2}. \tag{2.8}$$

$$V_{2,t\to\infty} = V\frac{R_2}{R_1+R_2} \tag{2.9}$$

Let the charge stored in each layer be Q_1 and Q_2, then at $t = 0$ the charges will be

$$Q_{1,t=0} \;=\; Q_{2,t=0} \;=\; C_1\,V_{1,t=0} \;=\; C_2\,V_{2,t=0} = \frac{C_1C_2}{C_1+C_2}V. \tag{2.10}$$

At $t \to \infty$ the charge stored in each layer will be,

$$Q_{1,t\to\infty} \;=\; C_1V_{1,t\to\infty} = \frac{C_1R_1}{R_1+R_2}V \tag{2.11}$$

$$Q_{2,t\to\infty} \;=\; C_2V_{2,t\to\infty} = \frac{C_2R_2}{R_1+R_2}V. \tag{2.12}$$

Hence, the change in charge storage from $t = 0$ to $t \to \infty$ in each layer can be given as,

$$\Delta Q_1 = (Q_{1,t\to\infty}) - (Q_{1,t=0}) = VC_1\frac{(R_1C_1 - R_2C_2)}{(R_1+R_2)(C_1+C_2)} \tag{2.13}$$

$$\Delta Q_2 = (Q_{2,t\to\infty}) - (Q_{2,t=0}) = VC_2\frac{(R_2C_2 - R_1C_1)}{(R_1+R_2)(C_1+C_2)}. \tag{2.14}$$

Therefore it is clear that the migration of charges occur only if $C_1R_1 \neq C_2R_2$. Since $C_1R_1 = \epsilon_0\epsilon_1\rho_1$ and $C_2R_2 = \epsilon_0\epsilon_2\rho_2$, charge migration can occur when an interface satisfies,

$$\epsilon_1\rho_1 \neq \epsilon_2\rho_2. \tag{2.15}$$

To the outside observer the two layer dielectric appears to be having an equivalent dielectric constant with real and imaginary parts $\epsilon^{'}$ and $\epsilon^{''}$ given by [16],

$$\epsilon^{'} = \frac{1}{C_0(R_1+R_2)}\frac{[(\tau_1+\tau_2) - \tau(1-\omega^2\tau_1\tau_2)]}{1+\omega^2\tau^2} \tag{2.16}$$

$$\epsilon^{''} = \frac{1}{\omega C_0(R_1+R_2)}\frac{[1-\omega^2\tau_1\tau_2 + \omega^2\tau(\tau_1+\tau_2)]}{1+\omega^2\tau^2}, \tag{2.17}$$

where $\tau_1 = R_1C_1$ and $\tau_2 = R_2C_2$ are the time constants of individual RC circuits mentioned in Figure 2.2. Also, the time constant of the equivalent circuit can be derived as $\tau = \frac{(C_1+C_2)R_1R_2}{R_1+R_2}$. Now, the static dielectric constant ϵ_s at $\omega = 0$ can be found using (2.16) as,

$$\epsilon^{'} = \epsilon_s = \frac{\tau_1 + \tau_2 - \tau}{C_0(R_1 + R_2)}, \tag{2.18}$$

where C_0 is the equivalent capacitance. The dielectric constant changes as the ω increases. When $\omega \to \infty$ we can show that,

$$\epsilon^{'} = \epsilon_\infty = \frac{\tau_1\tau_2}{\tau}\frac{1}{C_0(R_1 + R_2)}. \tag{2.19}$$

Using (2.18) and (2.19), the real and imaginary parts of the dielectric constants can be given as,

$$\epsilon^{'} = \epsilon_\infty + \frac{\epsilon_s - \epsilon_\infty}{1 + \omega^2\tau^2} \tag{2.20}$$

and

$$\epsilon^{''} = \frac{1}{\omega C_0(R_1 + R_2)} + \frac{\omega\tau(\epsilon_s - \epsilon_\infty)}{1 + \omega^2\tau^2}. \tag{2.21}$$

In reality there may be more than two interfaces, where all the interfaces which satisfy (2.15) will contribute to interfacial polarization and have an effect on the dielectric properties. This polarization mechanism is dominant for frequencies below 10 Hz.

When a particular dielectric is considered, several of these polarization mechanisms can coexist, thus the dielectric response is the result of the sum of these mechanisms. Although the polarization mechanisms illustrated in Figure 2.3 are distinguishable from each other, in reality these peaks can be broader and overlap, which means several polarization mechanisms can act at a given instance.

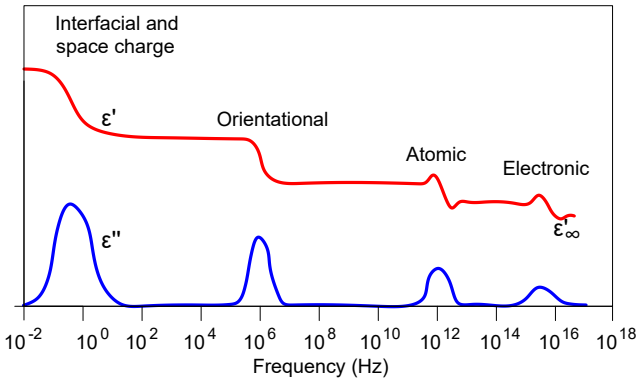

Figure 2.3. *A schematic representation frequency dependence of real and imaginary dielectric constant for different polarization mechanisms [16].*

2.3.2 Dielectric losses and dielectric constant

In the presence of an electric field, dielectric material will store energy by means of charge storage. The charge storing capacity or the capacitance depends on the different polarization mechanisms acting on the materials, which is represented by the dielectric constant. Consider a parallel plate capacitor with an area of A, thickness d filled with a dielectric having a dielectric constant ϵ. Then capacitance of the capacitor is defined by,

$$C = \frac{A\epsilon}{d}. \tag{2.22}$$

When the dimensions of the capacitor remain constant the capacitance only depends on the dielectric constant of the material. Hence the dielectric constant provides a measure of charge storing capacity of the material. For an electrical insulator the charge storage is undesirable, therefore materials with low dielectric constant is preferable. However, when a dielectric is subjected to an AC electric field the output current is changed by magnitude and phase. Therefore a dielectric insulation system result in a complex impedance. So the dielectric constant ϵ measured is also a complex

quantity,

$$\epsilon = \epsilon^{'} - j\epsilon^{''}. \tag{2.23}$$

Here, the real part $\epsilon^{'}$ contributes to energy storage as discussed earlier, whereas imaginary part $\epsilon^{''}$ contributes to the energy loss. In practice the dielectric constant is represented as a relative quantity (relative to the dielectric constant of air (ϵ_0), in other words relative permittivity or relative dielectric constant ϵ_r, which can be give by,

$$\frac{\epsilon}{\epsilon_0} = \epsilon_r = \epsilon_r^{'} - j\epsilon_r^{''}. \tag{2.24}$$

The energy loss occurs mainly due to continuous change in polarization of the dielectric in the presence of an alternating electric field. This is due to the fact that the change in polarization is not instantaneous but takes infinite time to decay [17]. The principal mechanism of energy loss is in the form of heat. This can be represented by a parallel equivalent circuit shown in Figure 2.4, where C is the lossless component and R is the heat emitting lossy component of the dielectric. Similarly, the AC loss can also be represented by a series equivalent circuit as per Figure 2.5.

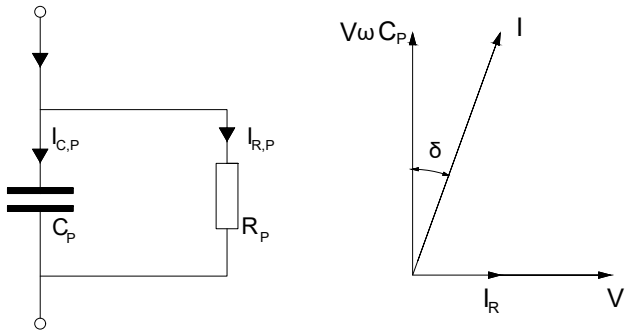

(a) *(b)*

Figure 2.4. *(a) Parallel equivalent circuit representation of a dielectric in the presence of an electric field (b) Vector diagram with loss angle δ.*

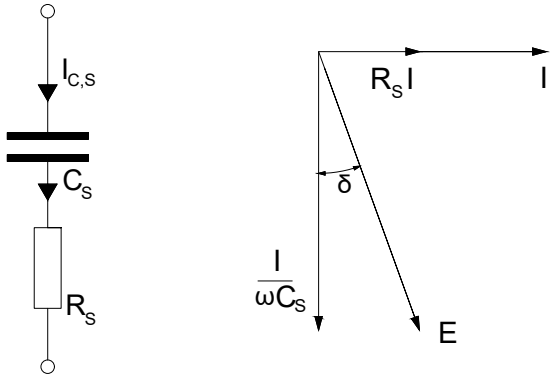

(a) *(b)*

Figure 2.5. *(a) Series equivalent circuit representation of a dielectric in the presence of an electric field (b) Vector diagram with loss angle δ.*

The dielectric losses can be represented by dissipation factor D [18],

$$D = tan\,\delta = \frac{1}{\omega C_P R_P} = \omega C_S R_S, \tag{2.25}$$

where C_P is the parallel capacitance, R_P is the parallel equivalent resistance, C_S is the series capacitance, R_S is series equivalent resistance, and $\omega = 2\pi f$ where f is the frequency in Hz. Also by definition [19],

$$tan\,\delta = \frac{\epsilon_r^{''}}{\epsilon_r^{'}} \tag{2.26}$$

Experimentally real relative dielectric constant can be found by [20],

$$\epsilon_r^{'} = \frac{C_k}{C_0}, \tag{2.27}$$

where C_k is the capacitance when the capacitor is filled with the dielectric and C_0 is the capacitance when filled by air. Hence, the imaginary relative permittivity can be found using (2.25) and (2.26).

Having discussed the theoretical background of dielectric constant and dielectric loss factor, we then summarize the dielectric constant values reported in recent literature of selected polymers in Table 2.2. The dielectric constant measurements depend on the measurement system, temperature and frequency of the AC signal. However, the measurement system to be used depends on the measurement frequency range and nature of the sample. Some of the measurement techniques available for dielectric constant measurement are parallel plate electrode methods (contacting and non-contacting), coaxial probe method, resonant cavity method and transmission line method. Since our experimental data are obtained through a parallel plate guard ring electrode system in room temperature 22 °C, we focus on summarizing similar results

from the wider research literature. A range of values are compared instead of a single value due to variations in results. Also, we found that, many researchers have reported complex dielectric constant instead of the loss tangent.

Table 2.2. *Dielectric constant and dielectric loss of selected polymers, AC at 1kHz*

Polymer	**Real Dielec.Cons.** $\epsilon_r^{'}$	**Imaginary Dielec.Cons.** $\epsilon_r^{''}$	**Loss tangent** $tan\,\delta$	**Reference**
PHB	2.2-2.6	0.02-0.09		[14], [21]
PHBV	2.42-2.77	0.05-0.06	0.03-0.01	[10], [22]
PCL	3.23-3.62	0.28-1.39	0.003-0.15	[10], [23]
PBS	4.59-5.08	0.012-0.087		[9], [13], [24]
PBAT	4.77-5.22	0.07-0.09		[10]
PLA	2.64-2.86	0.001-0.009	0.02	[9], [11]–[13], [24]
CA	4.5-8.6	0.08-0.11	0.002-0.09	[25]–[27]
LDPE	1.7-2.3	0.00006		[13], [24], [28], [29]
XLPE	1.87-2.3	0.001-0.06	0.004-0.04	[30]–[33]
PVC	3.29-3.5	0.06-0.1	0.013-0.1	[29], [34], [35]
EVA	2.4-3.8	0.01-0.3	0.007-0.06	[36]–[38]
NYLON 6	2.8-3.1	0.03-0.06	0.016-0.021	[39], [40]

2.3.3 Dielectric breakdown strength

Electrical breakdown is a critical limiting factor when polymers are used for electrical insulation applications. A key property attributable to this is the dielectric breakdown strength (DBS) of a polymer. DBS is the measure of maximum electrical field that the material can withstand without failure. The dielectric breakdown strength of polymers depend on many factors. Variation of thickness and homogeneity among samples even in different parts of the sample, voids and imperfections in the samples,

moisture and surface contamination, the electrode system being used, and the type of voltage application are some determining factors of experimental measurement of dielectric breakdown strength [41]. Also, the breakdown process in polymeric insulation materials are destructive and irreversible, hence only single measurement can be performed on a specific sample. So, it is important to evaluate electrical breakdown strength measurements in a similar setting when comparing the results.

Dielectric breakdown phenomena have been classified into several types using classical theories developed during the twentieth century. Mainly electronic, thermal, electromechanical and partial discharge breakdown mechanisms have been used to explain the breakdown phenomena [42]. The electronic structure of a polymer,

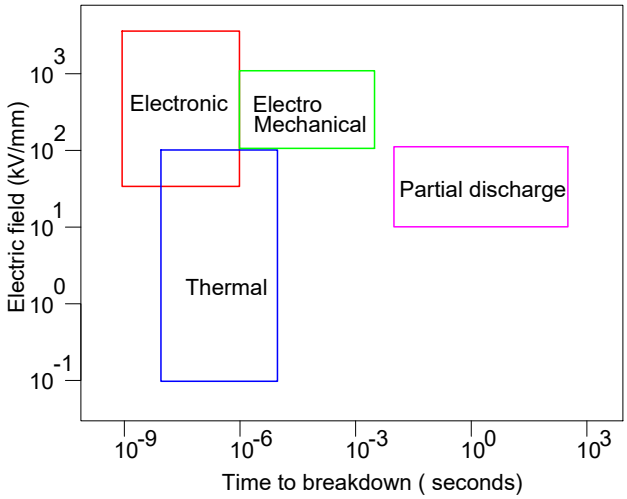

Figure 2.6. *Electric field and the time to breakdown of different electrical breakdown mechanisms [42].*

specifically its band gap between the valance and conduction bands has a direct effect on the DBS of a polymer. In a solid crystalline dielectric, the band structure represents the range of energies that an electron may have, therefore electrons can

only have energies in valence or conduction band. In such insulators the valance and conduction bands are separated by a large band gap. However, in polymeric insulation materials complete crystallinity is seldom achieved and more often they are amorphous or crystalline with local amorphous regions. Due to this structural arrangement, a large band gap is not well defined for polymers. There should be a correlation of the band gap of a polymer and its DBS, since an increased amount of energy is required to excite an electron from valence band to conduction band when the band gap is higher. However, this correlation is not simple as this phenomena also depend on the temperature [43].

Electronic breakdown occurs in a time of the order of 10^{-9} to 10^{-6} seconds. When a large electric field is applied to the dielectric, electrons gain energy which allows them to pass the energy gap from valence band to conduction band. This process is repeated as long as the electric field is present resulting in more and more conducting electrons, which eventually leads to breakdown of the dielectric. Sometimes these conduction electrons collide with other electrons liberating other electrons. When this process is repeated an electron avalanche is created, leading to electrical breakdown. There can be many avalanches forming at the same time extending through the entire thickness of the sample [44], [45].

Thermal breakdown occurs as a results of the conduction current and the local heat generated during conduction. Failure occurs when the rate of heat dissipation is lower than the rate of heat generation [41]. This phenomena is explained by the Joule's equation of electrical heating,

$$Q_j = I^2 R, \tag{2.28}$$

where Q_j is the heat generated, I is the conduction current, and R is the resistance

of the material. The temperature rise ΔT due to this heating can be derived by [41]

$$\Delta T = \pi V^2 \epsilon \tan\delta \, \rho \, f, \tag{2.29}$$

where V is the rms voltage, ϵ is the dielectric constant of the material, $tan\delta$ is the loss tangent, ρ is the thermal resistivity in °C.m/W and f is the frequency of the applied voltage. This rise in temperature eventually leads to breakdown of the material. Electrical stress due to conduction current and thermal stress due to temperature rise both act as the cause for dielectric breakdown.

Electromechanical breakdown occurs when the mechanical strength of the polymer decreases with temperature. At high temperatures, polymer dielectric materials start to soften. If the contacting electrodes are movable then, due to the electrostatic attraction, they will press the softening polymer dielectric and decrease the thickness. This will increase the electric field and lead to dielectric breakdown [42].

Gaseous inclusions in polymeric insulation are common under most manufacturing processes [46]. The gas inside the void has a lower dielectric constant than the surrounding media, hence electric field is intensified. This enhanced field cause the gases to ionize and discharge inside the void, but doesn't cause the whole polymer insulation to breakdown. However, the ionized gas is accelerated towards the polymer wall due to the electric field creating an erosion effect. When the insulation system is thin, this effect can cause complete electrical breakdown at a shorter time period. If the insulation system is thicker this partial discharges act as a insulation degradation mechanism [42].

In collating the dielectric breakdown strength (DBS) of selected polymers from research literature, it was found that many studies used ASTM D149 [8] standard for the measurement of dielectric breakdown strength. This standard specifies three

test methods, short-term-test, step-by-step, and slow rate-of-rise test. The standard also makes recommendations for the electrode system, surrounding media, voltage application method and statistical analysis are specified. The DBS of a material is measured by averaging at least five measurements of the breakdown voltage as per the standard. However, some researchers have also used Weibull statistical analysis to evaluate the DBS. This is a powerful statistical method in failure analysis. This method is useful when analysing larger sample sizes. When it comes to breakdown strength analysis of thin film polymer dielectrics most studies have used 20 or more samples. Weibull analysis is based on the cumulative probability of failure function $P(x)$ [47],

$$P(x) = \begin{cases} 1 - \exp(-[\frac{x-x_s}{x_0}]^{\beta}) & \text{for } x_s < x < \infty \\ 0 & \text{for } x < x_s \end{cases}$$

where x is the breakdown voltage or time-to-failure, x_s is the threshold voltage or threshold time and β is the scale parameter. The scale parameter of the Weibull plot is taken as the DBS [47], [48]. In this study we summarize DBS measurements using averaging. However, the breakdown strength data for many bio-based polymers appears not to be complete. Also, only a few researchers have explored the values reported in Table 2.3.

Table 2.3. *Dielectric strength of polymers studied for AC (at 50Hz), DC and Impulse voltage application. Statistical methods used for determining the breakdown strength, ave = average of multiple measurements, Wei = scale parameter of the Weibull distribution constructed from multiple measurements and max = maximum reading from multiple measurements.*

Polymer	**AC bd** (kV/mm)	**DC bd** (kV/mm)	**Impulse** (kV/mm)	**Reference**	**Remarks**
PHB					
PHBV		375	315	[23], [24]	ave
PCL					
PBS	279	276	412	[13], [24], [49]	ave
PBAT					
PLA	30/434	568	630	[13], [24], [49], [50]	ave / Wei
CA					
LDPE	18.5-28/425	406-478	359	[13], [24], [49], [51], [52]	ave
XLPE	22	496-620	467	[30], [33], [51], [53]–[55]	ave/Wei
PVC	24.5-60	65-84		[56]–[58]	max
EVA	20	347-380		[36], [59], [60]	ave / Wei
NYLON 6	16.6-34.8	570		[61]–[63]	ave/Wei

2.3.4 Volume resistivity

Volume resistivity of a polymer is measured generally by placing the sample between conductive electrodes. Then a DC electric field is applied to the electrodes. Even though an insulator should be resisting current flow, when a polymer sample is placed in an DC electric field a charging current is drawn from the sample due to the polarization phenomena explained earlier. This charging current drops gradually and settles at the leakage current point of the sample. The rate at which this initial current drop depends on the material and the polarization mechanisms in play. Next the resistance is calculated based on the ratio of voltage applied and the leakage current at steady state. Apart from the resistance of the sample the resistance measurement

depend on the applied voltage, electrode system and measurement time. So it is necessary to standardize these external factors for generalizing the results. ASTM D257 standard [64] specifies these parameters for a standardized resistivity measurement. This standard recommends a guard ring electrode system as illustrated in Figure 2.7. Coaxial cables are recommended for interconnections where the main lead is connected to the measurement circuit and the shield connected to the guard rings and ground. A DC voltage of 500V is recommended to be applied for a duration of 60 s, where the charging current is assumed to be settled at the said time. Upon the resistance measurement R_v, the volume resistivity is determined by

$$\rho = \frac{A}{t} R_v, \tag{2.30}$$

where A is the effective surface area calculated from the diameter D1 and D2 as shown in figure 2.7. The area (A) can be calculated by,

$$A = \frac{\pi(D_1 + D_2)^2}{16}. \tag{2.31}$$

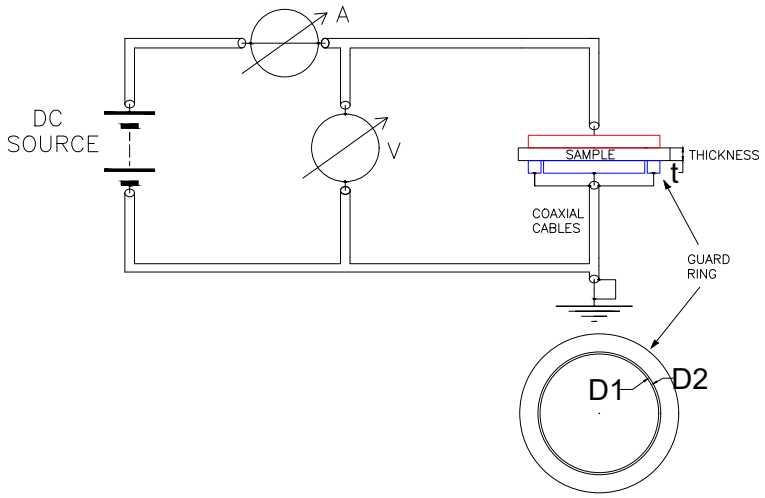

Figure 2.7. *Experimental setup recommended in ASTM D257 for volume resistivity measurement.*

Volume resistivity is measured in $\Omega\, m$ in SI units. This can be visualised as the electrical resistance through a unit volume as shown in Figure 2.8.

Electrical resistivity of material is an indirect indication of the dielectric breakdown strength (DBS) [64]. As the DBS measurements are always destructive, volume resistivity along with dielectric constant and loss tangent measurements can be used to predict an approximate insulation level while preserving the sample [65]. Like many other electrical properties, the volume resistivity is also dependent on the measurement temperature. With these concepts in mind we summarized volume resistivity measurements reported in recent literature in Table 2.4 for the selected polymers.

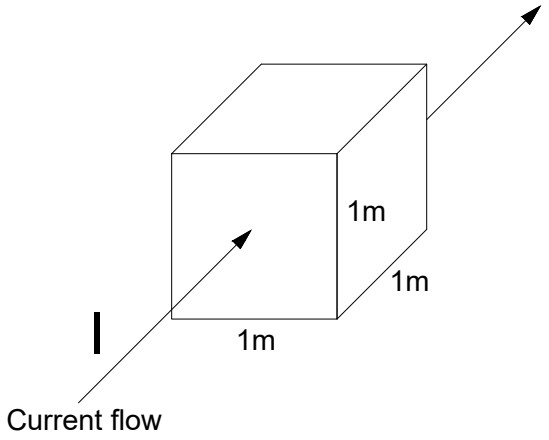

Figure 2.8. *Illustration of volume resistivity in terms of the resistivity through a unit volume.*

Table 2.4. *Volume resistivity measurements reported in literature obtained using ASTM D257.*

Polymer	**Vol.Res** $(\Omega\, m)$	**Reference**
PHB	10^{14}	[66]
PHBV	10^{14}	[67]
PCL	10^{9}	[10]
PBS	10^{10}	[10]
PBAT	10^{10}	[10]
PLA	$10^{14} - 10^{15}$	[10], [53]
CA	$10^{10} - 10^{11}$	[63], [68]
LDPE	$10^{13} - 10^{14}$	[51], [69]
XLPE	$10^{14} - 10^{15}$	[51], [70], [71]
PVC	$10^{9} - 10^{13}$	[71]–[73]
EVA	$10^{6} - 10^{11}$	[72], [74]
NYLON 6	$10^{10} - 10^{13}$	[67], [75]

2.4 Thermal properties

Before describing thermal properties of polymers and thermal analysis techniques, it is better to introduce several terms in thermodynamics. Let's start by introducing the heat flow, which is the amount of heat supplied per unit time, given by,

$$Heat\ \ flow = \frac{Heat}{Time} = \frac{q}{t}. \tag{2.32}$$

The heating rate is another important term which can be explained as the rate of change in temperature, which can be calculated from,

$$Heating\ \ rate = \frac{\Delta T}{t}. \tag{2.33}$$

The heat capacity (C_p) is the amount of heat required to raise the temperature by 1 ^0C. The heat capacity can be found by,

$$C_p = \frac{q/t}{\Delta T/t} = \frac{q}{\Delta T} \tag{2.34}$$

Thermal analysis is primarily based on the analysis of a materials response to heat. Among the wide variety of thermal analysis methods, differential scanning calorimetry (DSC) is the most common and widely used method [76]. ASTM D3418 standard specifies the DSC measurement procedure [77]. There are two main types of DSC techniques, heat flux and power compensated DSC. As illustrated in Figure 2.9, in a heat flux DSC the sample and reference are heated from the same heat source at a constant heating rate. The reference is usually kept empty while a measured quantity of sample is placed on the sample pan. Sample and reference are connected by a low-resistance heat-flow path, typically a metal disk. The temperature difference

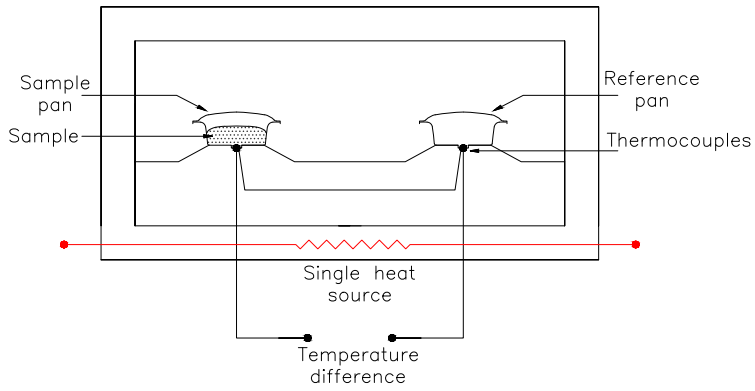

Figure 2.9. *Schematic diagram of heat flux DSC method.*

between the reference and sample is recorded and converted to heat using [78].

$$q = \frac{\Delta T}{R}, \tag{2.35}$$

where R is the thermal resistance of the heat flow path. Since the sample and reference are in good thermal contact, temperature of each remains same unless the sample undergoes a phase change, which change the heat capacity C_p.

In a power compensated DSC, the temperature of the sample and reference are controlled by two separate heat sources. Temperature of sample and reference are monitored individually and power input is controlled to keep both temperatures identical. The difference of power input is an indication of a phase change of the sample.

Temperature and the heat-flow obtained from DSC measurements is plotted in a heat-flow diagram as illustrated in Figure 2.11. There are three distinct temperatures that has a direct link with the physical properties of polymers as illustrated in Figure 2.11, namely the glass transition temperature T_g, and the melting temperature T_m,

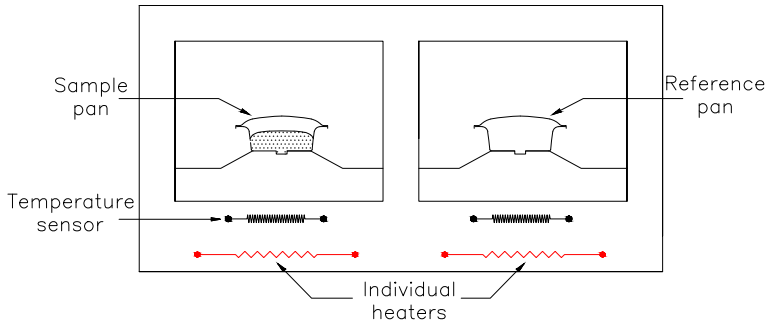

Figure 2.10. *Schematic diagram of power compensated DSC method.*

and crystallization temperature T_c. T_g is the temperature above which a polymer change from solid state to a rubbery state. This change occurs not at a distinct temperature, but over a range of temperatures. So, the T_g is taken as the center of the transition region. During glass transition electrical and mechanical properties of the material change dramatically. When temperatures increase above T_g the next physical transition occurs at the melting temperature T_m. At this temperature, the polymer transfers from a rubbery solid to complete liquid form. Similar to T_g, polymer melting occur gradually resulting in a range of melting temperatures and T_m is taken as the center of solid to liquid transition. Between (T_g) and (T_m), the material behaves as a rubber where it can be shaped or molded. At T_c, the molecules start to move and start to arrange into a systematic structure and crystallize. This transition is due to the previous processing history of the polymer. Specifically, this transition is clearly visible when the polymer lacks the sufficient time to crystallize during previous processing. This transition may be not visible in the next DSC heating cycle. Other than these temperatures, polymer materials can undergo other minor transi-

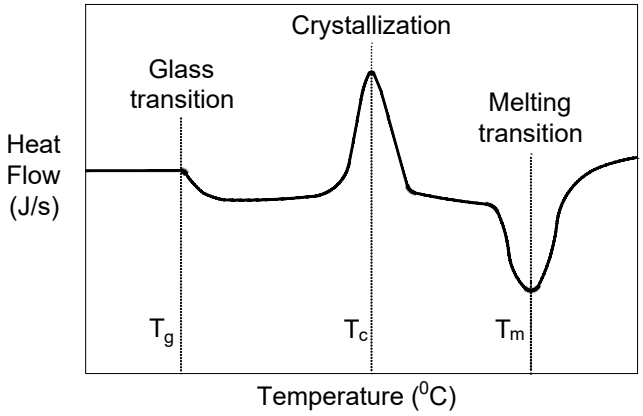

Figure 2.11. *Typical heat flow diagram of a polymer [79].*

tion temperatures, this is due to the fact that different regions of the polymer sample can have crystalline and amorphous regions at the same time. The systematically arranged molecular structure in the crystalline regions may undergo the phase transition at a different temperature compared to unevenly arranged amorphous region [80]. Having discussed the background of thermal analysis we now summarize the T_g and T_m of the selected polymers in Table 2.5.

Table 2.5. *Glass transition temperature T_g and melting temperature T_m of selected polymers obtained using DSC.*

Polymer	$T_g(^oC)$	$T_m(^oC)$	**Reference**
PHB	-30	170-179	[81]–[83]
PHBV	-17.6	108-112	[81], [82], [84]
PCL	-60/40	59-70	[81], [85], [86]
PBS	-30	114-127	[87], [88]
PBAT	-39	109-120	[89], [90]
PLA	50-60	130-180	[29], [81]
CA	185	230-290	[86], [91]
LDPE	-110	110-115	[81], [86]
XLPE	80	108	[32], [92], [93]
PVC	81-87	175-212	[29], [86]
EVA	45	71	[94]
NYLON 6	50-70	220-225	[29], [86]

2.5 Mechanical properties

The mechanical strength of a polymer is measured basically by measuring the deformation for applied stress. The deformation depends on the material being tested, temperature, applied stress, duration of the applied stress, stress application rate, and stress history. Hence, these conditions must be standardized to compare results among experiments. ASTM D638 [95] and ASTM D882 [96] are the commonly-referred standards for these measurements. However, ASTM D882 specifically addresses testing of thin film polymer samples with thickness less than 0.25 mm. ASTM D638 is for testing of plastic specimens of any thickness up to 14 mm. Mechanical strength is traditionally tested from stress-strain tests, whereas practically this is done by a tensile testing machine. Initially, polymer samples should be cut into a dumbbell shape using a sample cutter as specified in ASTM D6287 [97]. The thickness of samples should

be in the same range where a 10% tolerance is allowed. Next, as illustrated in Figure 2.12, the polymer sample is clamped to the testing machine and an extensometer is mounted on the sample to measure the elongation. Extensometer elongation measurement can be through contact, non-contact video or laser methods. The clamps are pulled apart by an actuator and the applied force is measured. A stress-strain

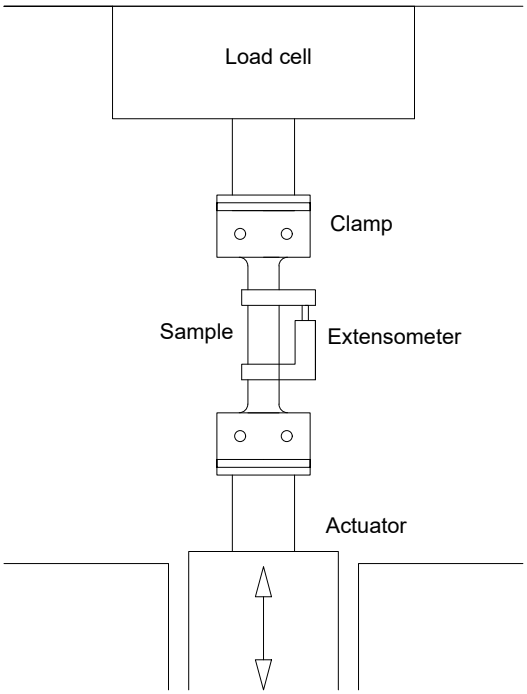

Figure 2.12. *Schematic diagram of a tensile testing machine [98].*

curve is generated form the measurements as illustrated in Figure 2.13.

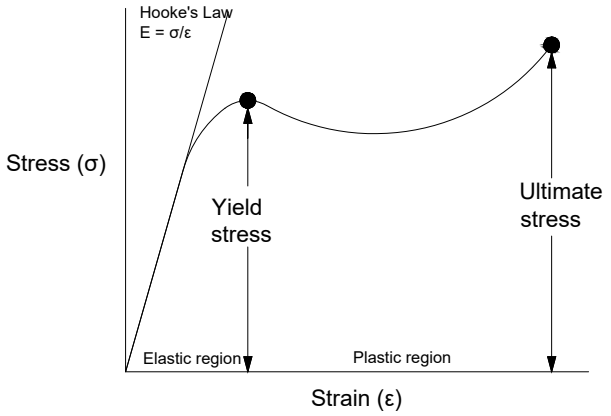

Figure 2.13. *Typical stress-strain curve of a polymer [99].*

Tensile stress is defined as,

$$Tensile\ stress\,(\sigma) = \frac{F}{A}, \tag{2.36}$$

where F is the force applied and A is the cross-sectional area as illustrated by Figure 2.14. Tensile strain is defined as,

$$Tensile\ strain\,(\epsilon) = \frac{\Delta L}{L_0}, \tag{2.37}$$

where ΔL is the elongation and L_0 is the original length.

To characterize the response to applied stress, tensile strength, percentage elongation at break, and Young's modulus are often calculated form the stress-strain curve. Tensile strength is the measure of force required to break the sample. Tensile strength is calculated by,

$$Tensile\ strength = \frac{Maximum\ load}{Original\ cross\text{-}section\ area}. \tag{2.38}$$

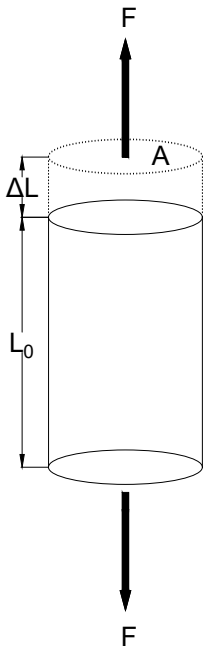

Figure 2.14. *Representation of tensile testing process.*

The tensile strength measurement depends on the sample geometry, sample preparation method, speed of the measurement, and the environment of testing. However, when these external factors are standardized, the tensile strength is directly linked to the chemical structure of the polymer: the higher the tensile strength, the tougher the polymer. But some polymers are weaker and soft, these polymers have low tensile strength and high percentage elongation values.

Percentage elongation at break indicates how much bending and shaping can be withstood by the material. Percentage elongation at break is calculated by,

$$Percentage\ elongation\ at\ break = \frac{Elongation\ at\ break}{Original\ length} \times 100\%. \tag{2.39}$$

During elongation, the material absorbs energy by plastic deformation. In the defor-

mation process, some of the energy is changed into heat and the rest is accounted for the change in orientation of the polymer molecules or creating cavities [86].

Another important mechanical property of polymers is the Young's modulus. Young's modules is the slope of the stress strain curve in the elastic region as illustrated by Figure 2.13. This characterizes materials response to low strain deformation. In low strain deformation material retain its original length upon releasing. The Young's modulus and tensile strength increase with molecular weight for glassy polymers.[100]. Next, we summarize these mechanical properties of the selected list of polymers from recent literature as reported in Table 2.6.

Table 2.6. *Mechanical properties tensile strength, percentage elongation to break and Young's modulus of selected polymers.*

Polymer	**Tensile strength** MPa	**Percentage elon.to break** %	**Young's modulus** GPa	**Reference**
PHB	40	1.5-5	1.6-3.5	[81], [82]
PHBV	19-38	5	0.6-2.9	[81], [82]
PCL	14-33	450-1100	0.4-0.2	[81], [101]–[103]
PBS	31	5	2	[87], [104]
PBAT	20-63	600-766	3.4	[89], [90]
PLA	53	16	3.45	[29], [81]
CA	26-41	24	1.1-1.3	[105], [106]
LDPE	9.7-17.2	500-725	0.16-0.36	[29], [81], [107]
XLPE	22	600	0.22	[108], [109]
PVC	55	40-80	2.8	[29]
EVA	6.2-28	73-78	0.01	[29], [110]
NYLON 6	80	30-100	2.6-3	[29], [86]

2.6 Summary

In this Chapter we considered the theoretical background of our research and summarized electrical, mechanical, and thermal properties of the selected polymers from recent research literature. We started our discussion by introducing the polymer materials we considered for the study and the rationale behind the selection. Research done on bio-polymer properties was found to be relatively new, therefore we explained the research contribution of two distinct groups, who has evaluated properties of multiple polymers in a similar setting in our literature search. Next, polymer properties were explained in detail, explaining the theoretical aspects and literature measurements. Having discussed these concepts, we then move on to describing the experimental procedures and properties measured from these experiments.

Chapter 3

Methodology

3.1 Sample preparation and raw materials

Sample preparation has a vital role on the experimental measurements. As discussed earlier, sample thickness and sample preparation methodology has an effect on the measurements of many material properties. Therefore, in our study we used samples prepared from a single method, and also with a similar thickness range for our measurements.

3.1.1 Sample preparation methodology

Samples were prepared from a spin caster custom built by the department of Biosystems Engineering, University of Manitoba. As shown in Figure 3.1, the instrument consists of a spinning platform (made out of a stainless steel disk) where the rotational speed can be controlled. The instrument has a rotational speed range of 500-1500 rpm. All polymer raw materials were purchased in the form of pellets. Table 3.1 shows the supplier of each polymer used for sample preparation. As the first step a known weight of polymer was completely dissolved in chloroform in room tempera-

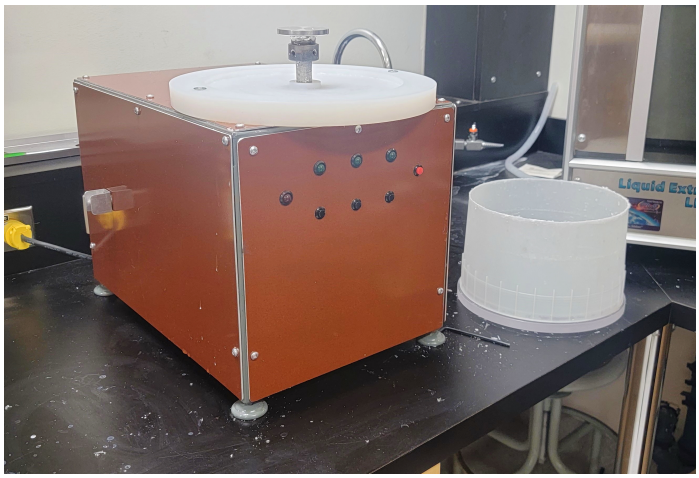

Figure 3.1. *Spin caster used to generate polymer samples*

ture. Solvents used and the supplier information is also reported in Table 3.1. To evenly distribute a polymer layer on the platform, 3-4 ml of the polymer solution was pipetted and spun on a set rotation speed for 1 minute. The rotation speed used to produce the sample was indicated on the sample numbering. For example, the first PLA sample produced with a solution having weight concentration of 10 % at 500 rpm was named as PLA(10)-500-1. The viscosity of the solution and the rotational speed determines the thickness of the films produced. The films were then air dried on the platform for 5 minutes, next platform is placed in a -20 ^0C freezer for easy removal of the films. Each sample was fabricated with one layer of spin cast materials. Thin samples were preferred to match testing requirements, specifically for the dielectric breakdown tests as the voltage source had maximum voltage limit of 20kV. Also, since the breakdown voltage range for many bio-polymers were unknown, single layer thin samples were employed for the measurements. Commercial forms of bio-polymers were used in sample preparation, whereas a supply of in-house bio-sourced materials was difficult to develop amidst the COVID-19 pandemic. Synthesis approaches and molecular structures for these polymers are presented in Appendix A.

Table 3.1. *Materials and solvents used for sample preparation and the supplier information*

Polymer	Supplier
PHB	Sigma-Aldrich
PHBV	Sigma-Aldrich
PCL	Sigma-Aldrich
PBS	Mitsubishi Chemical Corporation
PBAT	Global Polymers Corporation
PLA	Goodfellow Inc
Chloroform	Goodfellow Inc

3.2 Measured dielectric properties

3.2.1 Dielectric breakdown strength

Dielectric breakdown strength was tested by applying an electric field on the test material and measuring the maximum voltage that the material can withstand. The dielectric breakdown voltage depend on the thickness of the sample, shape of the electrodes, impurities and imperfections of the sample, method of voltage application (step-by-step or rate-of-rise) and voltage type (AC, DC or Impulse). However, the relative measurements of dielectric breakdown strength in a specific test setting is important to determine their usability as an electric insulator.

In our study we used a spherically capped electrodes of type VDE (Verband Deutscher Elektrotechniker) [111], as illustrated in Figure 3.2. The dimensional measurements of the electrodes are given in Figure 3.3. A finite element simulation in COMSOL multiphysics 5.6 was conducted to evaluate the behaviour of electric field between the electrodes. As shown in Figure 3.4, the maximum electrical field intensity is clearly focused at the center of the electrodes. This was beneficial as multiple

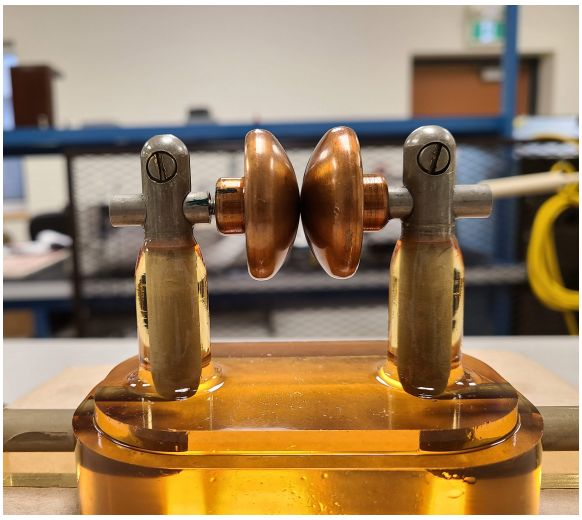

Figure 3.2. *Spherically capped VDE type electrodes*

measurements on each sample could be performed. This minimized any errors associated with variations in between samples. Also, we found that maximum electric field E at the center can still be calculated using the parallel plat formula (3.1),

$$E = \frac{V}{d}, \tag{3.1}$$

where V is the applied voltage and d is the electrode separation. As shown in Figure 3.5 for a terminal voltage of 1000 V and an electrode separation of 0.051 mm, we found that the maximum electrical field at the origin (0,0) is 19.6 kV/mm. Dielectric breakdown strength (DBS) was calculated using (3.1) and measured dielectric breakdown voltage.

As illustrated in Figures 3.6 and 3.7, a KEYSIGHT AC6802B AC power source with a current trip limit of 2 A was used. The generated voltage was stepped up from a oiled filled transformer with a ratio of 1:3000. This voltage was measured with a FLUKE 80K-40 HV voltage probe and a Hewlett Packard E2373A digital multi meter. The sample under test was mounted in between the VDE electrodes and fixed

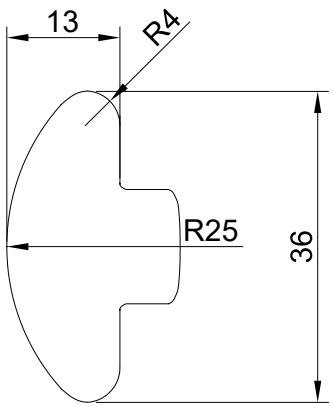

Figure 3.3. *Dimensions of a VDE type spherically capped electrode used in the study. All dimensions are in millimeters.*

at a 0.051 mm distance. This fixed distance was set using a thickness gauge. This gap was sufficient enough for all polymer samples to be placed in between electrodes without compressing. Polymer films were fixed in place using electrical insulating adhesive tapes pasted to the rear of the electrode. The assembly was then held in air and a 60 Hz AC voltage was applied using the step-by-step method as specified in ASTM D149. The minimum voltage step was 36 V whereas the time step used was 20 s or till a stable voltage was visible at the source.

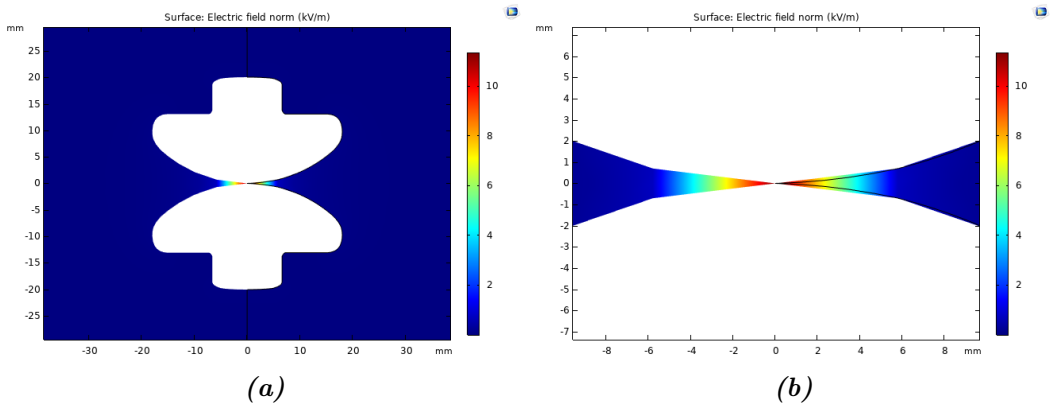

Figure 3.4. *Electric field distribution simulated from COMSOL multiphysics, (a) Cross-section taken from the X-Z plane, (b) Close-up view of the electric field pattern at the origin (0,0).*

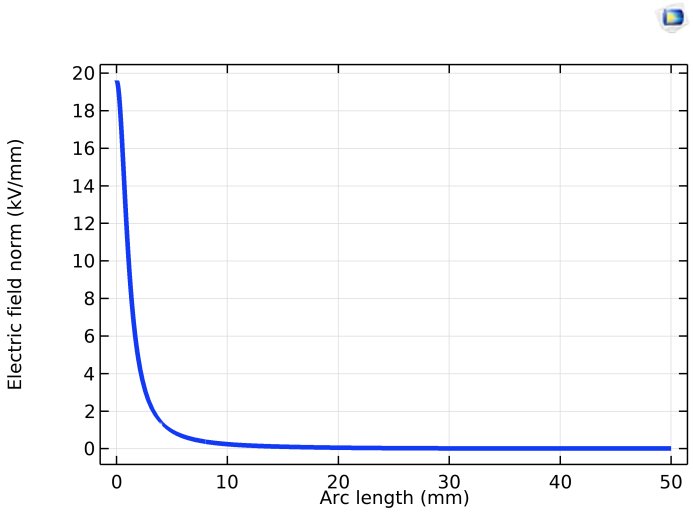

Figure 3.5. *Variation of electric field E radially from the origin shown in Figure 3.2.*

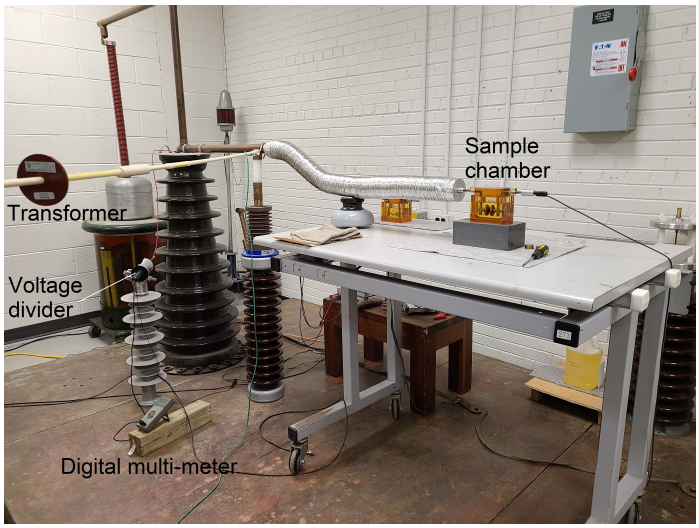

Figure 3.6. *Test setup including step-up transformer, voltage divider, digital multimeter and sample chamber.*

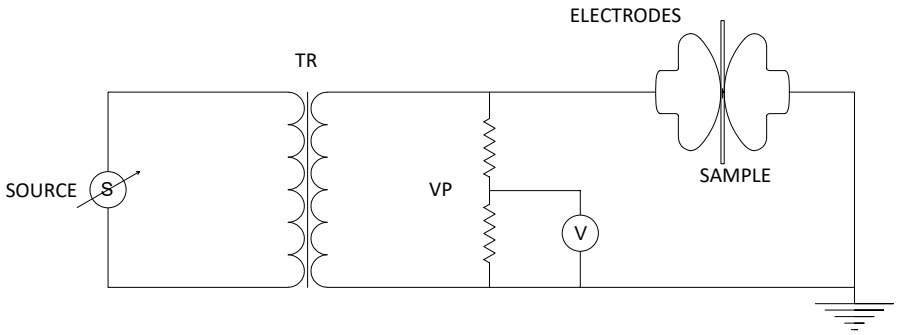

Figure 3.7. *Test schematic including AC variable voltage source (S), step-up transformer (TR), voltage probe (VP), digital multimeter measuring the AC voltage (V) and the sample placed in between the spherically capped electrode system.*

3.2.2 Dielectric spectroscopy

The dielectric constant or relative permittivity of a material consists of real (ϵ') and imaginary (ϵ'') components as highlighted in (2.23). The real part of dielectric constant or the real relative permittivity of a material is useful to determine the charge storing capacity of a material. The imaginary part of the dielectric constant is related to the dielectric loss. When used as an electrical insulator it is desirable to have less capacitance. Therefore, materials with low dielectric constant is preferred. This is clear from equation (3.2) for the relationship between capacitance and dielectric constant of a ideal parallel plate capacitor. In both instances energy loss is undesirable, therefore low imaginary permittivity is always preferred.

$$C = \frac{A\epsilon}{d} \tag{3.2}$$

In the study, the dielectric constant measurements were completed using a Solartron ModulabXm Material Testing System. As illustrated in Figure 3.9, the instrument consists of a variable frequency power source and a complex voltage and current measuring system. The sample was mounted on a guard ring electrode system with an electrode diameter of 10 mm. The guard ring electrode system minimizes the erroneous capacitance measurements that can occur due to fringing field effect of a parallel plate capacitor. The diameter of the electrode assembly with the guard ring was measured 55 mm. Hence the samples were sized approximately at 60 mm. Upon mounting, the thickness of the sample is measured using the micrometer assembly available on the sample holder as shown in Figure 3.8. Five thickness measurements were taken rotating each sample to five random positions. Dielectric measurements were done using the average thickness of these five readings. In the experiment real and imaginary relative permittivity of the sample was measured while varying the

frequency from 1 to 100 kHz. The voltage applied during the measurement was 8 V, and no physical damage was expected during the measurements. All measurements were done at room temperature measured 22 °C.

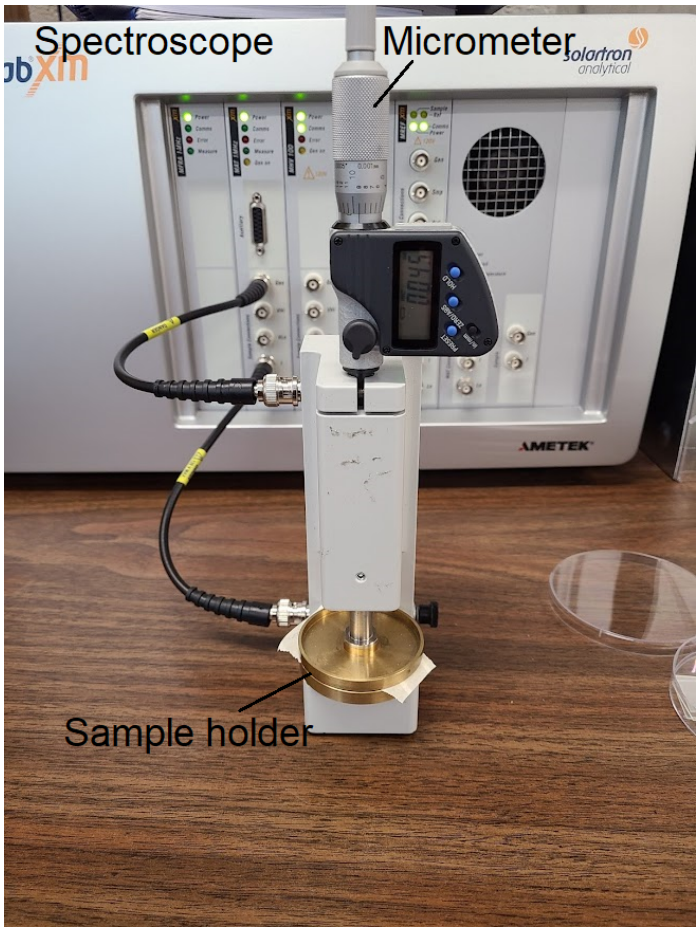

Figure 3.8. *Solartron 12962 A micrometer sample holder system*

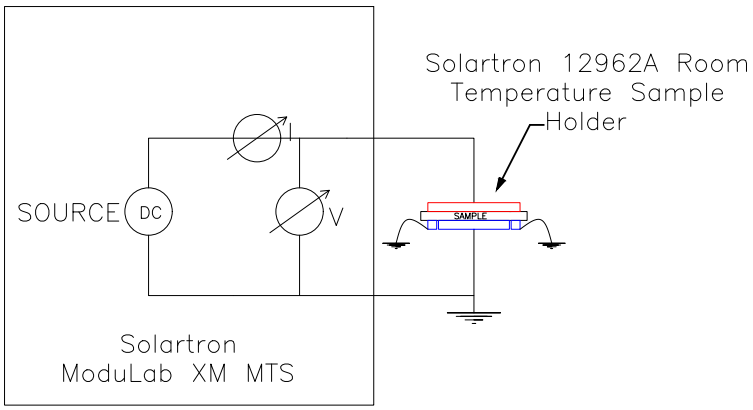

Figure 3.9. *Simplified circuit diagram of Solartron Modulab XM MTS and sample holder connection.*

3.2.3 Volume resistivity

Solartron XM High voltage module coupled with XM Femto ammeter module was used to measure the volume resistance of the samples. Samples were mounted on to the Solartron 12962 A micrometer sample holder system. The fixed electrode of 30 mm diameter (equipped with a guard ring and an overall diameter of 55 mm similar to movable electrode) was used for the measurements. DC voltage of 100 V was applied for 60 s and the resistance at the end of the time period was recorded. The volume resistivity was calculated from,

$$\rho = \frac{A}{t} R_v, \tag{3.3}$$

where ρ is the volume resistivity, A is the area, t is thickness of the sample and R_v is the resistance measured at the 60th second while applying the DC voltage. Area A of the guard ring electrode is measured as ,

$$A = \frac{\pi(D_1 + D_2)^2}{16}. \tag{3.4}$$

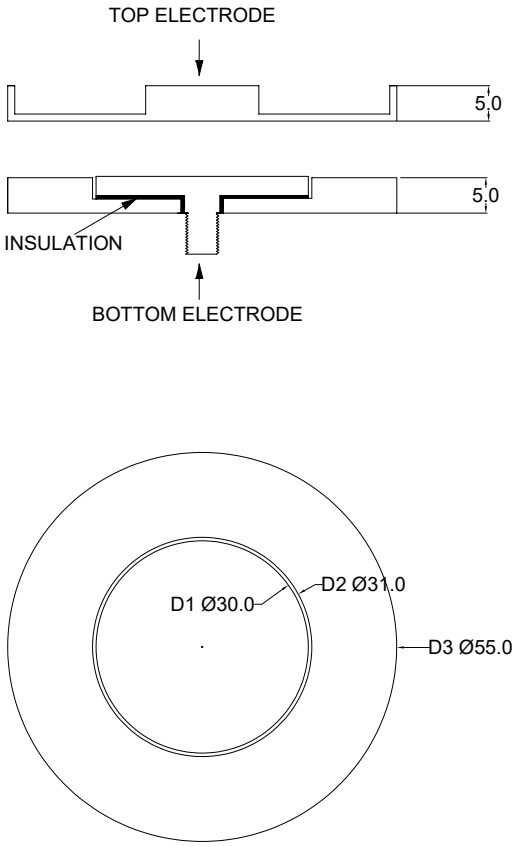

Figure 3.10. *Dimensions of the Solartron 12962 A guard ring electrode system*

ASTM D257 [64] and IEC 62631 [112] are the common standards that specify the standard criteria for volume resistivity measurement. The standard recommends a guard ring electrode system with an overall diameter of 100 mm or 50 mm. The DC voltage to be applied is recommended as 100V or 500V. However, in our study we used above mentioned Solartron measurement system with an overall diameter of 55mm and a DC voltage of 100V. As reported in Appendix B.3, the thickness was averaged using five consecutive readings taken while rotating the sample. All measurements were done at room temperature measured 22 °C.

3.3 Summary

We conducted electrical measurements including dielectric spectroscopy, AC breakdown tests, and volume resistivity measurements on the samples. These samples were prepared by a spin casting process developed by the department of Biosystems Engineering. Samples consisted of a single layer with a thickness range of 20-40 μm. Dielectric spectroscopy measurements were done using Solartron ModulabXM MTS. AC breakdown test was done using a spherically capped electrode system in air complying with ASTM D149 [8] standard. Volume resistivity measurements were done using the XM High voltage module and XM Femto ammeter module of the Solartron ModulabXM MTS. All these measurements were taken in room temperature at 22 °C. Having described the measurement methodologies, now let's move onto discussing the obtained results from these measurements.

Chapter 4

Results and Discussion

4.1 Summary of Dielectric properties

4.1.1 Dielectric breakdown strength (DBS) measurements

With our study on DBS, we can now compare the performance of selected bio-polymers with their fossil-fuel-based counterparts. As described in Chapter 3, the AC breakdown strength of bio-polymers PHB, PHBV, PCL, PBS, PBAT and PLA was measured experimentally complying ASTM D149 [8]. Since these measurements were obtained in a similar setting, they are directly comparable with each other. As shown in Figure 4.1, from these measurements PHB, PCL, PBAT, and PLA have significantly higher AC breakdown strength, which is comparable with XLPE and PVC. PHBV shows the lowest AC breakdown strength which is significantly lower than all other polymers studied. The complete data set of AC breakdown strength measurements obtained during this study is tabulated in Appendix B.2.

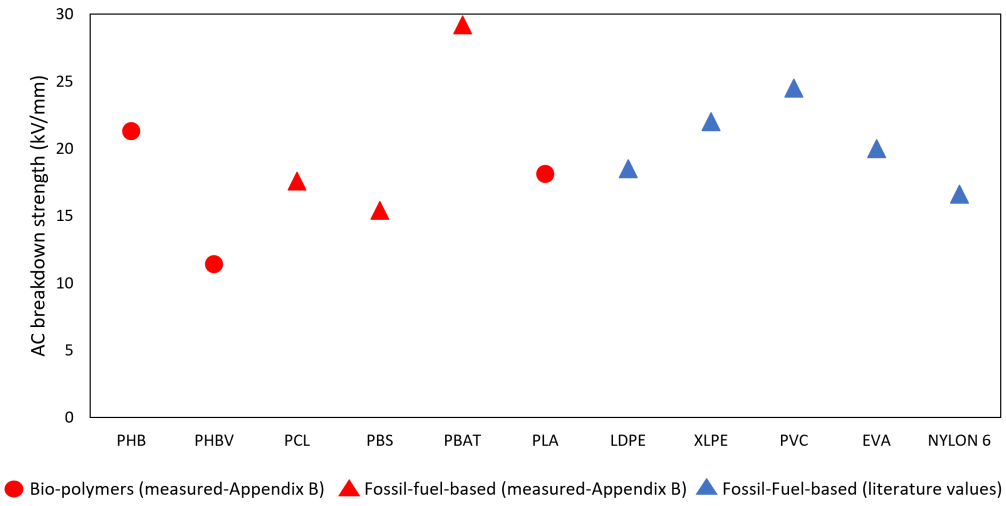

Figure 4.1. *AC (60Hz) breakdown strength of selected polymers at room temperature 22 °C. The complete set of measurement values are provided in Appendix B.2.*

However, as mentioned in Table 4.1, the AC breakdown strength values reported in [23], [24], [49] on PBS, PLA, and LDPE vary significantly from our experimental values, as well as values reported in other sources, specifically Li, Guo, Wen-Dong, *et al.* [50] and Notinger and Stancu [51]. However, these values were obtained using a different setup, specifically a McKeown-type electrode systems were used in their experiments where the two electrodes and the sample sheet were fixed with epoxy resin and then immersed in silicone oil. This doesn't comply with ASTM D149 [8] standard. All other AC breakdown measurements summarized in Table 4.1, as well as our study follow ASTM D149 with different recommended electrode systems.

Table 4.1. *Dielectric strength of polymers studied for AC (at 50Hz/60Hz), DC and Impulse voltage application. Statistical methods used for determining the breakdown strength, ave = average, Wei = scale parameter of the Weibull distribution and max = maximum. Experimental results from this study are shown in red.*

Polymer	**AC bd** (kV/mm)	**DC bd** (kV/mm)	**Impulse** (kV/mm)	**Reference**	**Remarks**
PHB	21.3				ave
PHBV	11.4	375	315	[23], [24]	ave
PCL	17.6				ave
PBS	15.4/279	276	412	[13], [24], [49]	ave
PBAT	29.2				ave
PLA	18.1/30/434	568	630	[13], [24], [49], [50]	ave / Wei
CA					
LDPE	18.5-28/425	406-478	359	[13], [24], [49], [51], [52]	ave
XLPE	22	496-620	467	[30], [33], [51], [53]–[55]	ave/Wei
PVC	24.5-60	65-84		[56]–[58]	max
EVA	20	347-380		[36], [59], [60]	ave / Wei
NYLON 6	16.6-34.8	570		[61]–[63]	ave/Wei

Direct current (DC) breakdown strength values summarized in Table 4.1 are much higher than the AC breakdown strength values. It is known that the DC breakdown strength of a material is twice or higher than the AC breakdown strength [113]. Also, this phenomena is present in many insulating materials in the form of thin films or thick boards [114]–[118]. However, this is not fully-explained in the current research literature. One explanation for this phenomena involves space charge measurements in the presence of AC and DC electric fields. The difference in AC and DC breakdown strength is attributed to the difference in space charge distribution in the presence of AC and DC electric fields [113]. Under AC stress both positive and negative charges are accumulated on the material surface closer to the electrodes. These charges distort the applied electric field and lead to lower breakdown strength. In contrast, homo-charges are formed in the bulk of the materials in the presence of a DC electric field.

All-in-all, the AC breakdown is initiated at the electrode material interface whereas DC breakdown is initiated at the bulk of the material. Hence, the difference in DBS for AC and DC electric fields.

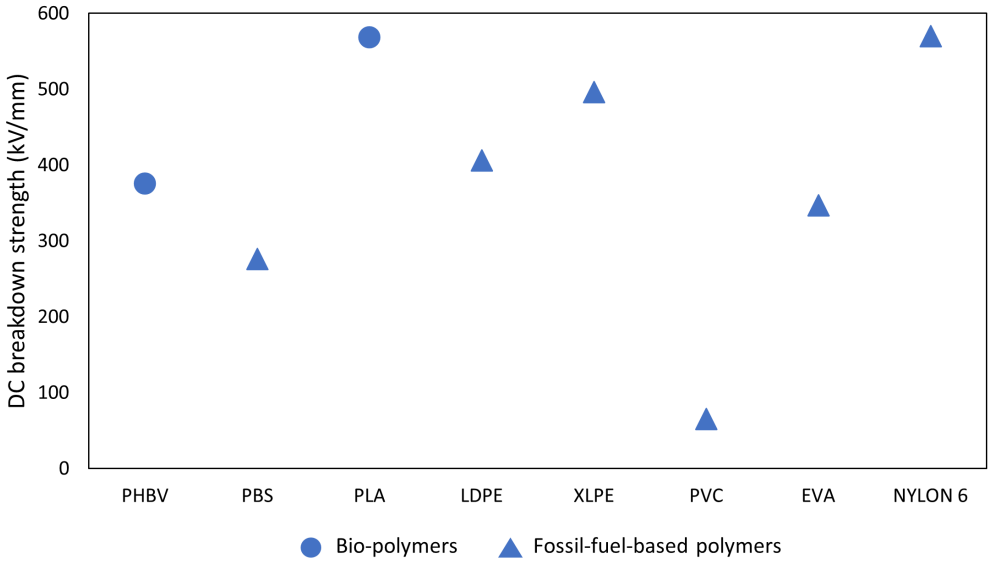

Figure 4.2. *DC breakdown strength of selected polymers at room temperature 22 °C. Data from literature sources described in Table 4.1.*

Measurements of the DC breakdown strength of bio-polymers is less common in research literature, whereas only PHBV, PBS and PLA has been investigated. However, the DC breakdown strength of these polymers are comparable with conventional fossil-fuel-based polymers as illustrated in Figure 4.2. PLA shows the highest DBS which is in the range with XLPE. PHBV and PBS has a lower DBS which is comparable with EVA.

There were only a handful of comparable impulse breakdown strength measurements available in the research literature, as illustrated in Figure 4.3. However, from the available measurements, PLA shows significantly higher impulse breakdown strength, which is comparable with XLPE. Impulse breakdown strength of PBS and

PHBV were lower but in the same range as LDPE.

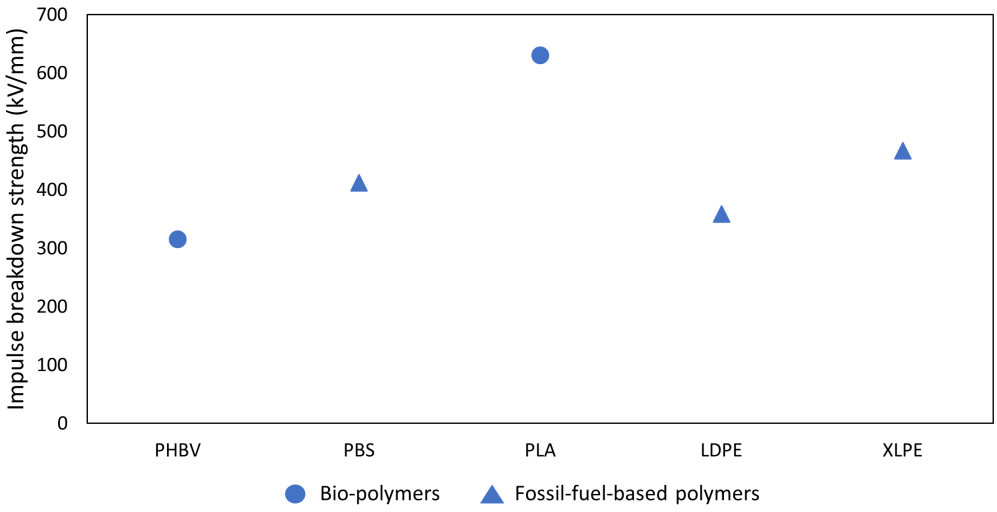

Figure 4.3. *Impulse breakdown strength of selected polymers at room temperature 22 °C. Data from literature sources described in Table 4.1.*

4.1.2 Complex relative permittivity measurements

Considering the real relative permittivity measurements summarized in Table 4.2, we can see that the PHB, PCL, PBS, PBAT and PLA data closely follow the range of values reported in the literature. However, PHBV shows significantly higher range compared to that reported in the literature. This is probably due to different hydroxyvalerate content in the samples. As reported in Appendix B, the samples measured in our experiment had a hydroxyvalerate content of 20% weight, whereas the measurements reported in [10], [22] has a hydroxyvalerate content of 8% weight. Since the measurements reported in Table 4.2 were measured with the same electrode system in a similar setting, these measurements are directly comparable with each other. Also, the accuracy of the measurements are validated from the measurements reported in literature. A complete set of measurement data on the real and imaginary dielec-

Table 4.2. *Comparison of the real part of dielectric constant $\epsilon_r^{'}$ and the imaginary part of dielectric constant $\epsilon_r^{''}$ measured in this study (for a frequency range of 1 to 100kHz) with values reported in recent literature.*

Name	Measured		Reported in literature		Source
	$\epsilon_r^{'}$	$\epsilon_r^{''}$	$\epsilon_r^{'}$	$\epsilon_r^{''}$	
PHB	2.11-2.5	0.0026-0.067	2.2-2.6	0.02-0.09	[14], [21]
PHBV	3.09-4.45	0.006-0.204	2.42-2.77	0.05-0.06	[10], [22]
PCL	2.95-3.78	0.00004-0.43	3.23-3.62	0.28-1.39	[10], [23]
PBS	4.51-5.12	0.0001-0.47	4.59-5.08	0.012-0.087	[9], [13], [24]
PBAT	4.58-5.13	0.001-0.37	4.77-5.22	0.007-0.09	[10]
PLA	2.14-2.92	0.00007-0.33	2.64-2.86	0.001-0.009	[9], [11]–[13], [24]

tric constant are available in Appendix B.1. In this study, a broad frequency range was considered in order to explore the range of dielectric properties a material would exhibit. This is important as the voltage/current wave-forms in power systems are often contaminated with high frequency harmonics and impulses [119]. The behaviour of the dielectric material to a broad range of frequencies is therefore important to understand the limitations of the dielectric.

As described in Chapter 2, when the dielectric is used as an insulator, higher values of dielectric constant $\epsilon^{'}$ are undesirable. Therefore, the highest point in the measurements are the critical points for comparison. Also, the imaginary dielectric constant is linked with the loss factor, thus lower the value the better the material. Hence, we considered highest values of imaginary dielectric constant as the critical point. Figure 4.4 was generated based on these critical measurement points, whereas CA, LDPE, XLPE, PVC and EVA were plotted based on the highest values reported in literature. Therefore, for electrical insulation applications polymers in the lower left-hand side are desirable. In fact, we can see that XLPE, LDPE, PVC, NYLON 6,

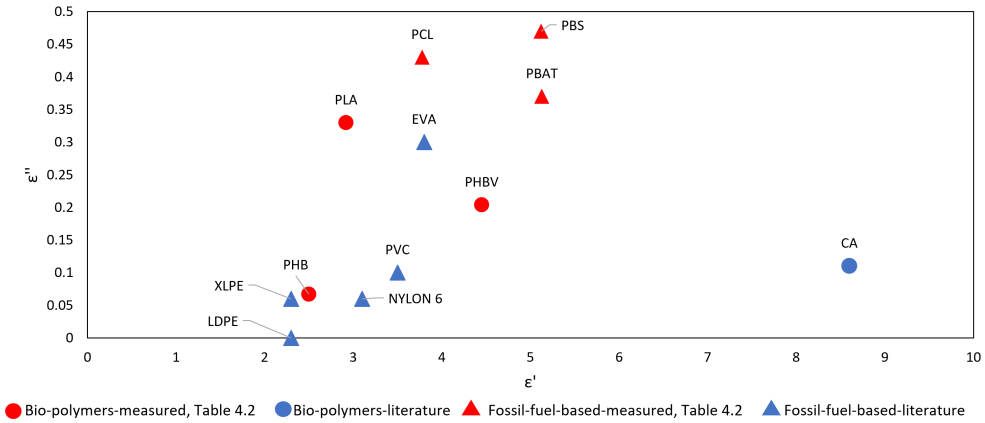

Figure 4.4. *Placement of polymers with reference to the real and imaginary dielectric constant measured at room temperature 22 °C in a frequency range of 1Hz to 100kHz, based on data provided in Tables 4.2 and 2.2.*

and PHB are in this region. Hence, PHB can be identified as a potential candidate considering its dielectric properties.

4.1.3 Volume resistivity

As described in Chapter 3, volume resistivity was measured using the Solartron ModuLab XM MTS in room temperature recorded as 22 °C. From Table 4.3, we can see that the measured values are higher than the values reported in the literature. This is due to the different electrode systems and different measurement voltages used. Specifically, PCL, PBS. and PBAT have significantly higher resistivity compared to literature values. However, literature values for these three polymers were obtained from the same literature source [10], whereas the volume resistivity ρ ($\Omega\, m$) was calculated using the reported conductivity values σ(S/m) using the relationship $\rho = 1/\sigma$. In [10], conductivity values were obtained using Al foil electrodes of the diameter 20 mm (without any guard ring arrangement). They used conduction current at the end of 1000 s for conductivity calculation. There was no mention of the applied DC

voltage during the measurement. However, in our measurements we used a guard ring electrode system with a electrode diameter of 30mm, and applied 100 V for 60 s end of which the resistance was measured directly. Also, the Solartron micrometer sample holder that we used in our experiment is equipped with a ratchet stop mechanism to apply a constant measurement pressure. Therefore, our resistance measurements are independent from the errors due to varying measurement pressure. Volume resistivity was calculated using these resistance values and the volume involved in the measurement. The complete table of resistance values obtained during this study are available in Appendix B.3. Due to the change in measurement procedure, literature values for PCL,PBS and PBAT are not directly comparable with the measured values. However, since PHB, PHBV, PCL, PBS, PBAT and PLA were measured in the same setup, our experimental measurements are directly comparable with each other.

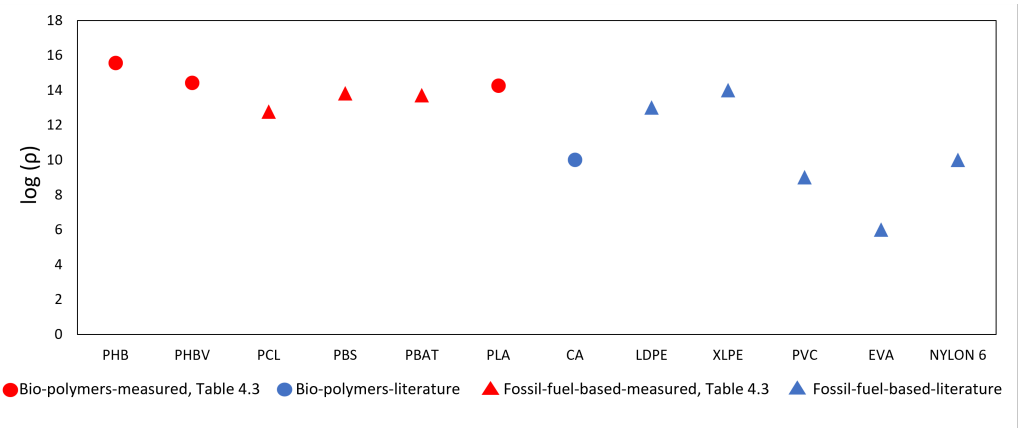

Figure 4.5. *Comparison of log(ρ) values for selected polymers (original volume resistivities recorded in Ωm), based on measurement data tabulated in Table 4.3 and literature data tabulated in Table 2.4.*

Figure 4.5 was generated from the logarithmic values of volume resistivity measurements. From Figure 4.5 and Table 4.3 we can see that PHB has the highest volume resistivity, whereas PHBV, PCL, PBS, PBAT, PLA also show relatively high volume resistivity values.

Table 4.3. *Comparison of volume resistivity (ρ) measurements with values reported in recent literature.*

Name	Measured ($\Omega\, m$)	Reported in literature ($\Omega\, m$)	Source
PHB	3.60×10^{15}	10^{14}	[66]
PHBV	2.63×10^{14}	10^{14}	[67]
PCL	5.89×10^{12}	10^{9}	[10]
PBS	6.57×10^{13}	10^{10}	[10]
PBAT	5.15×10^{13}	10^{10}	[10]
PLA	1.79×10^{14}	$10^{14} - 10^{15}$	[53]

4.2 Summary of Thermal properties

During our previous discussions in Chapter 2, we identified three important transition temperatures of a polymers, specifically glass transition T_g, crystallinity temperature T_c and melting temperature T_m. Of these transitions, we analyse T_g and T_m of selected polymers as T_c is more dependent on the material processing. As described in Chapter 2, if the material is allowed sufficient time during processing, the crystallinity process would occur uninterruptedly and T_c transition would not be visible during Differential Scanning Calorimetry (DSC) measurements. Figure 4.6 was generated from T_g and T_m values obtained in literature tabulated in table 2.5. For electrical insulation applications, materials with high T_g and T_m are preferred. This is evident as the fossil-fuel-based conventional electrical insulation materials XLPE, PVC, NYLON 6 and EVA are in the top right hand corner of Figure 4.6. PCL, PBAT, PBS, PHB and PHBV show lower T_g values and can be compared with LDPE. CA shows the best thermal performance as it has very high T_g and T_m. However, CA is known to have high electrical losses and lower volume resistance as discussed previously. PLA, on

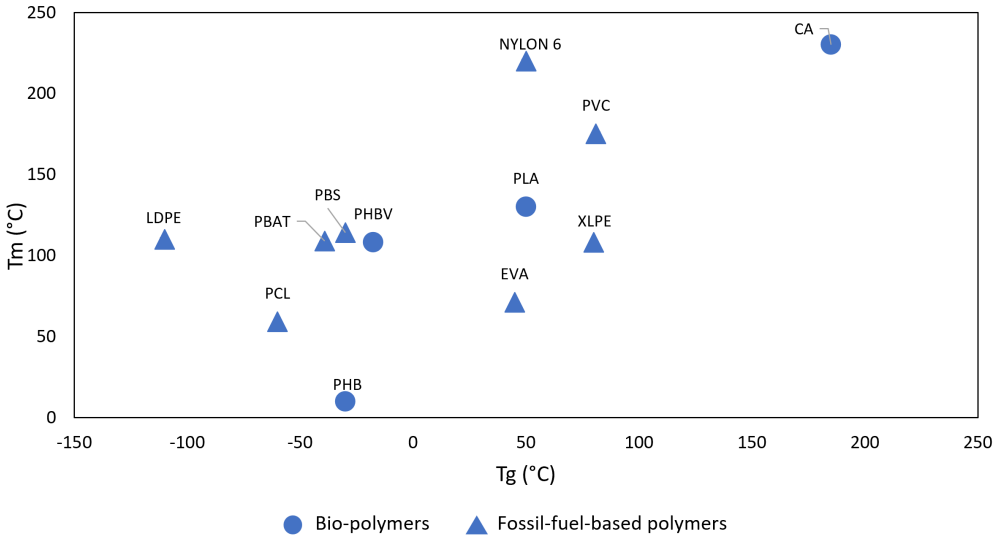

Figure 4.6. *Comparison of glass transition (T_g) and melting (T_m) temperature of selected polymers.*

the other hand is close, to the conventional polymers considering thermal properties and also PLA shows good dielectric and electrical breakdown properties.

4.3 Summary of Mechanical properties

4.3.1 Tensile strength

Tensile strength indicates the maximum force a material can withstand without mechanical failur,e as discussed in Chapter 2. Therefore, higher tensile strength is desirable for practical applications. As illustrated in Figure 4.7, NYLON 6 has the highest tensile strength ($\sim$ 80 MPa). This is important within electrical cables, as the outer layer is made of NYLON 6 sheath. PHB and PLA show moderately high tensile strength which is comparable with PVC. PCL and PBAT show lower tensile strength, which can be compared with LDPE and XLPE. PCL and PBAT have good

AC breakdown strength which is also comparable with LDPE and XLPE. However, dielectric performance of PCL and PBAT needs improvement as they have higher values for real and imaginary dielectric constant.

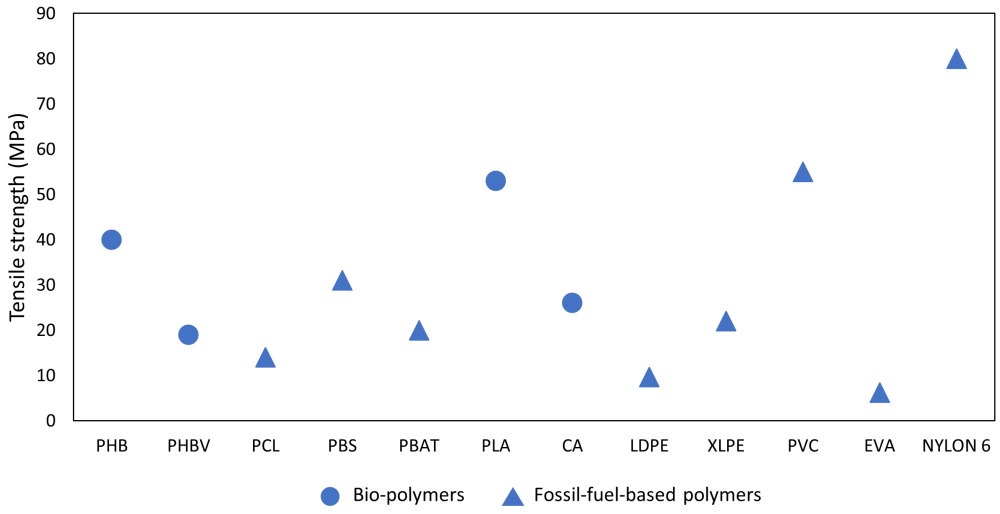

Figure 4.7. *Tensile strength of selected bio-polymers and fossil-fuel-based polymers obtained from recent literature summarized in Table 2.6.*

4.3.2 Percentage elongation at break

Percentage elongation is an indication of how well a material behaves during plastic deformation. Considering an electrical insulation application for an electrical cable, low elongation is desirable for outer sheaths such as PVC and NYLON 6 as a pulling force is applied directly to these layers during cable handling. High elongation is suitable for inner layers as elongations and contractions during cable bending should be absorbed by these inner layers. However, percentage elongation at break values summarized from literature show a large variation among the polymers studied. PCL and PBAT shows higher values in the range of 400-600 %, which is comparable with LDPE and XLPE. PBS, CA, PHB. and PLA have lower values which are comparable

with PVC, EVA and NYLON 6. PHBV shows lower tensile strength as well as lower elongation at break, thus seems mechanically weak than other polymers studied.

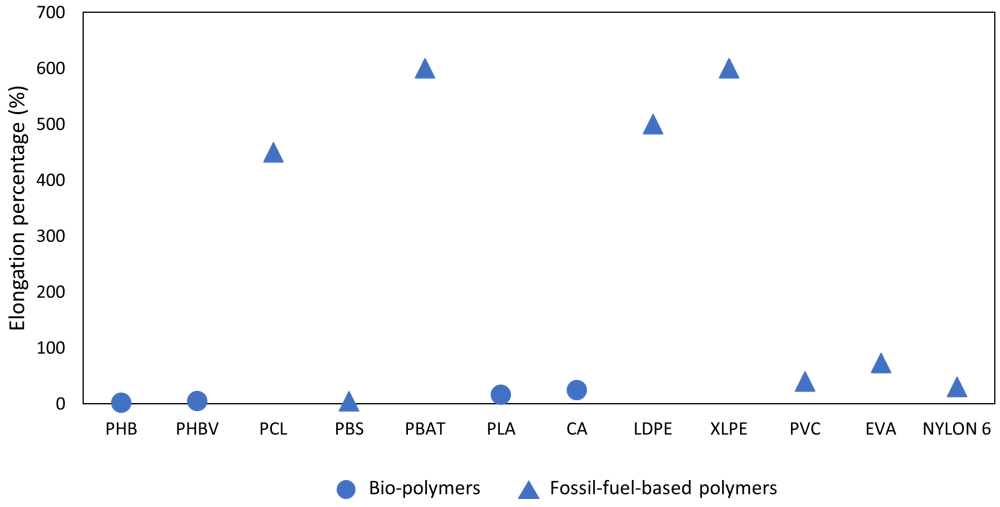

Figure 4.8. *Percentage elongation at break of selected bio-polymers and fossil-fuel-based polymers obtained from recent literature.*

4.3.3 Young's modulus

Young's modulus is an important property as it indicates the materials ability to withstand changes in length and return to its original values. This is important considering an electrical cable application since the cable should be able to withstand minor length changes and return to its original length when the pulling force during handling is released. Therefore, higher Young's modulus is desirable for an electrical cable. PLA, PBAT, PHB and PBS shows higher Young's modulus, which is comparable with PVC and NYLON 6. PHBV and PCL have lower Young's modulus, which can be compared with LDPE and XLPE.

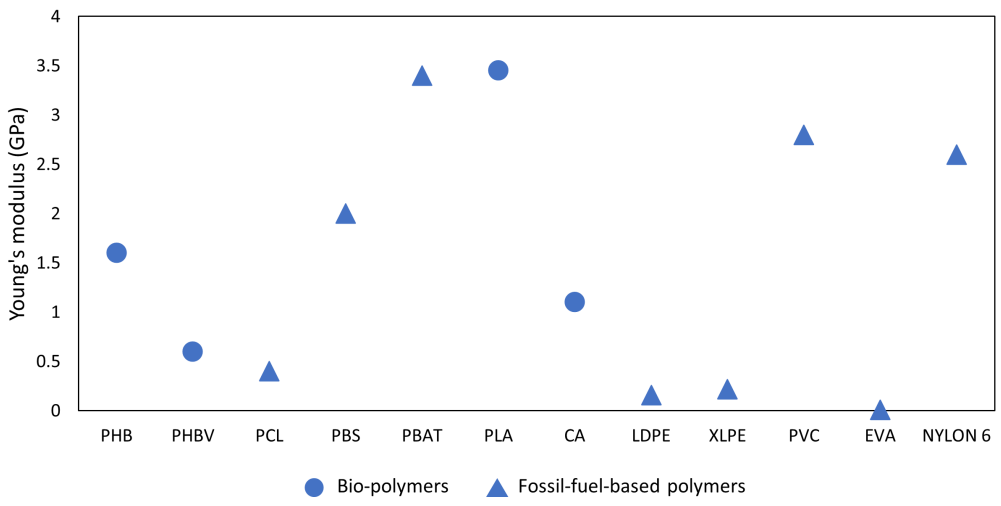

Figure 4.9. *Young's modulus of selected bio-polymers and fossil-fuel-based polymers obtained from recent literature.*

4.4 Summary

In this Chapter we critically analysed material properties obtained from literature data as well as from experimental measurements. Important electrical, mechanical and, thermal properties of the selected set of polymers were compared. Electrical properties such as complex dielectric constant, dielectric breakdown strength, and volume resistivity were also compared. For thermal properties, glass transition temperature, and melting temperature were analysed. Finally, for mechanical properties, tensile strength, percentage elongation at break, and Young's modulus were compared.

Chapter 5

Conclusions

In this thesis a systematic approach was presented for replacing fossil-fuel-based polymeric insulation materials with bio-polymers. In order to do this, electrical, mechanical and thermal properties of selected set of polymers are researched. As the first step, the theoretical background of each property as well as the standards used for measurements were explained. Next, measurements for each of these properties are summarized from recent literature. Based on this investigation, it is evident that the dielectric breakdown strength (DBS) of many bio-polymers are unknown and a benchmarking is incomplete without these measurements. Also, it is clear that other electrical properties including dielectric constant and volume resistivity of the selected bio-polymers should be measured in a similar test setting to achieve a meaningful comparison. This is because these measurements are highly dependent on the test procedure and ambient conditions.

Several bio-polymers can be identified as potential candidates to substitute fossil-fuel-based polymers, from the analysis of experimental results and literature data. PHB shows promising results including good AC breakdown strength (> 20 kV/mm), excellent dielectric performance (low real and imaginary dielectric constant), very high

volume resistivity ($> 10^{15}\,\Omega\,m$), compared to its fossil-fuled-based counterparts LDPE and XLPE. However, PHB needs a certain improvement in mechanical and thermal properties. PHB has a low glass transition temperature T_g and melting temperature T_m as well as very low elongation percentage at break, all of which needs further improvement. This is possible through thermal treatment and annealing, blending with tougher polymers and chemical cross linking processes [120], [121]. PHB has a moderate tensile strength and a moderate Young's modulus, which is favourable for practical use. PCL, PBS and PBAT have excellent AC breakdown strength, good volume resistivity, but all three show poor dielectric performance (high real and imaginary dielectric constant) and poor thermal performance. PHBV has poor AC breakdown strength as well as poor thermal and mechanical properties. Therefore, PHBV is not suitable for electrical insulation applications. Also, CA has poor dielectric performance, low volume resistivity and poor mechanical strength. Dielectric breakdown strength of CA is unknown to date. However, due to unfavourable properties mentioned above CA is deemed unfit for electrical insulation applications. Considering all, PLA has good AC breakdown strength ($\sim$ 25 kV/mm), excellent DC ($\sim$ 500 kV/mm) and impulse ($\sim$ 600 kV/mm) breakdown strength, moderate dielectric performance, excellent volume resistivity ($\sim 10^{14}\,\Omega\,m$), excellent thermal properties and good mechanical properties.

Therefore, PLA can be shortlisted as a suitable candidate for electrical insulation applications. Also, PHB can be identified as a possible candidate for further improvement, whereas the thermal properties should be improved to suite electrical insulation applications.

5.1 Summary of main findings

- AC breakdown strength of polymers PHB, PHBV, PCL, PBS, PBAT and PLA was measured for the first time, complying ASTM D149 standard [8].
- Comparison of electrical, thermal, and mechanical properties of bio-polymers as well as conventional fossil-fuel-based polymers was conducted systematically. Advantages and disadvantages of each polymer were identified clearly.
- Considering the overall performance, PLA was found to be a suitable candidate material to substitute fossil-fuel-based polymeric electrical insulation materials.
- PHB was identified to be a suitable candidate for further improvement.

5.2 Future works

Finally, we plan the following as a future extension of this research:

- Conduct DC and impulse breakdown tests on the selected bio-polymers as well as fossil-fuel-based polymers using a larger sample size.
- Conduct additional AC breakdown tests using a large sample size and calculate the breakdown strength using Weibull analysis.
- Conduct resistivity measurements with different electrode systems, such as Al film, or conductive paint to identify their dependence.
- Develop polymer blends, composites or identify chemical cross-linking pathways to improve mechanical properties of PHB.

References

[1] K. Mathes, "A brief history of development in electrical insulation," in *[1991] Proceedings of the 20th Electrical Electronics Insulation Conference*, IEEE, 1991, pp. 147–150.

[2] J. Mead, Z. Tao, and H. Liu, "Insulation materials for wire and cable applications," *Rubber chemistry and technology*, vol. 75, no. 4, pp. 701–712, 2002.

[3] K. Barber and G. Alexander, "Insulation of electrical cables over the past 50 years," *IEEE Electrical Insulation Magazine*, pp. 27–32, 2013.

[4] R. Vogelsang, O. Sekula, H. Nyffenegger, and W. Weissenberg, "Long-term experiences with XLPE cable systems up to 550 kV," *Konferenka Siovenskih Electroenergetikov–Kranjska Gora*, 2009.

[5] W. A. Thue, *Electrical power cable engineering*. Boca Raton, FL 33487-2742, USA.: CRC Press, 2017, pp. 217–235.

[6] K. Casey, *The Coming Chaos: Fossil Fuel Depletion and Global Warming*. Dorrance Publishing, 2018.

[7] J. P. Greene, *Sustainable plastics: environmental assessments of biobased, biodegradable, and recycled plastics*. John Wiley & Sons, 2014.

[8] "ASTM D149-20, standard test method for dielectric breakdown voltage and dielectric strength of solid electrical insulating materials at commercial power frequencies," ASTM International, West Conshohocken, PA, Standard, 2018.

[9] Y. Ohki and N. Hirai, "Electrical conduction and breakdown properties of several biodegradable polymers," *IEEE Transactions on Dielectrics and Electrical Insulation*, vol. 14, no. 6, pp. 1559–1566, 2007.

[10] N. Hirai, H. Ishikawa, and Y. Ohki, "Electrical conduction properties of several biodegradable polymers," in *2007 Annual Report-Conference on Electrical Insulation and Dielectric Phenomena*, IEEE, 2007, pp. 592–595.

[11] K. Shinyama and S. Fujita, "Study on the electrical properties of a biodegradable plastic," in *Proceedings of the 7th International Conference on Properties and Applications of Dielectric Materials (Cat. No. 03CH37417)*, IEEE, vol. 2, 2003, pp. 707–710.

[12] Y. Maeno, H. Kino, S. Omori, N. Hirai, T. Tanaka, Y. Ohki, Y. Tajitsu, M. Kohtoh, and S. Okabe, "Dipolar polarization and depolarization currents in biodegradable polymers," in *Proceedings of 2005 International Symposium on Electrical Insulating Materials, 2005.(ISEIM 2005).*, IEEE, vol. 2, 2005, pp. 417–420.

[13] V. Hegde, O. Gallot-Lavallée, and L. Heux, "Overview on thermal and electrical properties of biodegradable polymers," in *2015 IEEE 11th International Conference on the Properties and Applications of Dielectric Materials (ICPADM)*, IEEE, 2015, pp. 540–543.

[14] O. Gallot-Lavallée and L. Heux, "Dielectric spectroscopy on a PHBV biopolymer," in *2013 Annual Report Conference on Electrical Insulation and Dielectric Phenomena*, IEEE, 2013, pp. 559–562.

[15] K. W. Wagner, "Erklärung der dielektrischen nachwirkungsvorgänge auf grund maxwellscher vorstellungen," *Archiv für Elektrotechnik*, pp. 371–387, 1914.

[16] G. G. Raju, "Chapter 4 : Dielectric loss and relaxation—II," in *Dielectrics in electric fields: Tables, Atoms, and Molecules*, Boca Raton, FL 33487-2742, USA: CRC press, 2017, pp. 137–182.

[17] ——, "Chapter 3 : Dielectric loss and relaxation—I," in *Dielectrics in electric fields: Tables, Atoms, and Molecules*, Boca Raton, FL 33487-2742, USA: CRC press, 2017, pp. 83–136.

[18] A. J. Ruys, *Alumina Ceramics: Biomedical and Clinical Applications*. Sawston, Cambridge, England.: Woodhead Publishing, 2018, p. 424.

[19] "ASTM d150-18, standard test methods for ac loss characteristics and permittivity (dielectric constant) of solid electrical insulation," ASTM International, West Conshohocken, PA, Standard, 2018.

[20] A. Scott and H. L. Curtis, "Edge correction in the determination of dielectric constant," *Journal of research of the National Bureau of Standards*, vol. 22, p. 747, 1939.

[21] A. Kotp and M. Ahmed, "Dielectric and electric modulus of poly (3-hydroxybutyrate) semi-crystalline polymer," *International Journal of Polymeric Materials*, vol. 57, no. 12, pp. 1075–1082, 2008.

[22] T. Fahmy, M. Ahmed, A. El-Kotp, H. Abdelwahed, and M. Alshaeer, "Broadband dielectric spectroscopy and electric modulus analysis of poly (3-hydroxybutyrate-co-3-hydroxyvalerate) and related copolymers films," *International Journal of Physics and Applications*, vol. 8, pp. 1–14, 2016.

[23] V. Hegde, "Dielectric study of biodegradable and/or bio-based polymeric materials," Ph.D. dissertation, Université Grenoble Alpes, 2017.

[24] N. Hirai and Y. Ohki, "Dielectric properties of biodegradable polymers," in *2006 IEEE Conference on Electrical Insulation and Dielectric Phenomena*, IEEE, 2006, pp. 668–671.

[25] K. Deshmukh, M. B. Ahamed, R. R. Deshmukh, S. K. Pasha, K. K. Sadasivuni, A. R. Polu, D. Ponnamma, M. A.-A. AlMaadeed, and K. Chidambaram, "Newly developed biodegradable polymer nanocomposites of cellulose acetate and al 2 o 3 nanoparticles with enhanced dielectric performance for embedded passive applications," *Journal of Materials Science: Materials in Electronics*, vol. 28, no. 1, pp. 973–986, 2017.

[26] A. Sharma and C. Ramu, "Dielectric properties of solution grown cellulose acetate thin films," *Materials Letters*, vol. 11, no. 3-4, pp. 128–132, 1991.

[27] V. Veeravazhuthi, S. K. Narayandass, and D. Mangalaraj, "Dielectric behaviour of pure and nickel-doped cellulose acetate films," *Polymer international*, vol. 45, pp. 383–388, 1998.

[28] M. Ramanujam, V. Wachtendorf, P. J. Purohit, R. Mix, A. Schönhals, and J. F. Friedrich, "A detailed dielectric relaxation spectroscopy study of artificial UV weathered low density polyethylene," *Thermochimica acta*, pp. 73–78, 2012.

[29] J. Brandrup, E. H. Immergut, E. A. Grulke, A. Abe, and D. R. Bloch, *Polymer handbook*. Wiley New York, 1999.

[30] M. Roy, J. Nelson, R. MacCrone, L. S. Schadler, C. Reed, and R. Keefe, "Polymer nanocomposite dielectrics-the role of the interface," *IEEE transactions on dielectrics and electrical insulation*, pp. 629–643, 2005.

[31] E. Linde, L. Verardi, D. Fabiani, and U. Gedde, "Dielectric spectroscopy as a condition monitoring technique for cable insulation based on crosslinked polyethylene," *Polymer Testing*, pp. 135–142, 2015.

[32] J. Li, X. Zhao, G. Yin, S. Li, J. Zhao, and B. Ouyang, "The effect of accelerated water tree ageing on the properties of xlpe cable insulation," *IEEE Transactions on Dielectrics and Electrical Insulation*, pp. 1562–1569, 2011.

[33] V. Vahedy, "Polymer insulated high voltage cables," *IEEE Electrical Insulation Magazine*, pp. 13–18, 2006.

[34] X. Yu, B. Yi, F. Liu, and X. Wang, "Prediction of the dielectric dissipation factor tan δ of polymers with an ann model based on the dft calculation," *Reactive and Functional Polymers*, pp. 1557–1562, 2008.

[35] N. Srivastava, V. Sachdev, and R. Mehra, "Investigation of electrical and dielectric properties of prelocalized graphite/poly (vinyl chloride) composites near the percolation threshold," Wiley Online Library, 2007, pp. 2027–2033.

[36] A. M. Henderson, "Ethylene-vinyl acetate (EVA) copolymers: A general review," *IEEE Electrical Insulation Magazine*, vol. 9, no. 1, pp. 30–38, 1993.

[37] X. Huang, L. Xie, Z. Hu, and P. Jiang, "Influence of BaTiO 3 nanoparticles on dielectric, thermophysical and mechanical properties of ethylene-vinyl acetate elastomer/BaTiO 3 microcomposites," *IEEE Transactions on Dielectrics and Electrical Insulation*, pp. 375–383, 2011.

[38] X. Huang, L. Xie, P. Jiang, G. Wang, and F. Liu, "Electrical, thermophysical and micromechanical properties of ethylene-vinyl acetate elastomer composites with surface modified BaTiO3 nanoparticles," *Journal of Physics D: Applied Physics*, p. 245 407, 2009.

[39] L. Yun-Ze, L. Meng-Meng, S. Wan-Mei, K. Qing-Shan, and Z. Lei, "Electrical, dielectric and surface wetting properties of multi-walled carbon nanotubes/nylon-6 nanocomposites," *Chinese physics B*, p. 1221, 2009.

[40] A. Bizet, N. Nakamura, Y. Teramoto, and T. Hatakeyama, "Measurement of dielectric properties of polymers using fourier analysis," *Thermochimica acta*, pp. 147–157, 1994.

[41] G. G. Raju, "Chapter 13 : Breakdown in solid dielectrics.," in *Dielectrics in electric fields: Tables, Atoms, and Molecules*, Boca Raton, FL 33487-2742, USA: CRC press, 2017, pp. 573–619.

[42] L. A. Dissado and J. C. Fothergill, *Electrical degradation and breakdown in polymers*. London, United Kingdom: Peter Peregrinus Ltd., 1992, pp. 62–64.

[43] J. Bicerano, *Prediction of polymer properties*. Boca Raton, Florida, USA: CRC Press, 2002, pp. 327–329.

[44] A. Von Hippel, "Electric breakdown of solid and liquid insulators," *Journal of Applied Physics*, vol. 8, no. 12, pp. 815–832, 1937.

[45] L. Zhao, J. C. Su, and C. L. Liu, "Review of developments on polymers' breakdown characteristics and mechanisms on a nanosecond time scale," *AIP Advances*, vol. 10, no. 3, p. 035 206, 2020.

[46] G. Stevens, E. Perkins, and J. Champion, "Microvoid formation and growth in epoxy resins under mechanical and electrical stress by laser light scattering," in *1988 Fifth International Conference on Dielectric Materials, Measurements and Applications*, IET, 1988, pp. 234–237.

[47] C. Chauvet and C. Laurent, "Weibull statistics in short-term dielectric breakdown of thin polyethylene films," vol. 28, IEEE, 1993, pp. 18–29.

[48] L. Wang, H. Luo, X. Zhou, X. Yuan, K. Zhou, and D. Zhang, "Sandwich-structured all-organic composites with high breakdown strength and high dielectric constant for film capacitor," *Composites Part A: Applied Science and Manufacturing*, pp. 369–376, 2019.

[49] M. Matsushita, Y. Maeno, H.-r. Kino, S. Fujita, N. Hirai, T. Tanaka, Y. Ohki, Y. Tajitsu, M. Kohtoh, and S. Okabe, "Effects of glass transition on the dielectric breakdown and electrical conduction in several biodegradable polymers," in *Proceedings of 2005 International Symposium on Electrical Insulating Materials, 2005.(ISEIM 2005).*, IEEE, 2005, pp. 413–416.

[50] X.-R. Li, J. Guo, L. Wen-Dong, L.-Y. Zhang, C. Wang, B.-H. Guo, and G.-J. ZHANG, "Analysis of morphology and electrical insulation of 3d printing parts," in *2018 IEEE International Conference on High Voltage Engineering and Application (ICHVE)*, IEEE, 2018, pp. 1–4.

[51] P. Notinger and C. Stancu, "Failure mechanisms in XLPE," in *Crosslinkable Polyethylene: Manufacture, Properties, Recycling, and Applications*, Gateway East, Singapore 189721, Singapore.: Springer Nature, 2021, p. 272.

[52] C. Zhou and G. Chen, "Space charge and ac electrical breakdown strength in polyethylene," *IEEE Transactions on Dielectrics and Electrical Insulation*, pp. 559–566, 2017.

[53] T. Nakagawa, T. Nakiri, R. Hosoya, and Y. Tajitsu, "Electrical properties of biodegradable polylactic acid film," *IEEE Transactions on Industry Applications*, vol. 40, no. 4, pp. 1020–1024, 2004.

[54] J. Wu, H. Jin, A. R. Mor, and J. Smit, "The effect of frequency on the dielectric breakdown of insulation materials in hv cable systems," in *2017 International Symposium on Electrical Insulating Materials (ISEIM)*, IEEE, 2017, pp. 251–254.

[55] B. Du, *Polymer Insulation Applied for HVDC Transmission*. Springer Nature, 2021.

[56] A. Thabet and N. Salem, "Experimental verification on dielectric breakdown strength using individual and multiple nanoparticles in polyvinyl chloride," *Transactions on Electrical and Electronic Materials*, pp. 274–282, 2020.

[57] A. Laifaoui, M. S. Herzine, Y. Zebboudj, J.-M. Reboul, and M. Nedjar, "Breakdown strength measurements on cylindrical polyvinyl chloride sheaths under ac and dc voltages," *IEEE Transactions on Dielectrics and Electrical Insulation*, pp. 2267–2273, 2014.

[58] S. A. Mansour, R. Elsad, and M. Izzularab, "Dielectric spectroscopic analysis of polyvinyl chloride nanocomposites loaded with Fe2O3 nanocrystals," *Polymers for Advanced Technologies*, pp. 2477–2485, 2018.

[59] G. C. Montanari, D. Fabiani, F. Palmieri, D. Kaempfer, R. Thomann, and R. Mulhaupt, "Modification of electrical properties and performance of EVA and PP insulation through nanostructure by organophilic silicates," *IEEE Transactions on Dielectrics and Electrical Insulation*, pp. 754–762, 2004.

[60] M. Hikita, T. Hirose, Y. Ito, T. Mizutani, and M. Ieda, "Investigation of electrical breakdown of polymeric insulating materials using a technique of pre-breakdown current measurements," *Journal of Physics D: Applied Physics*, vol. 23, no. 12, p. 1515, 1990.

[61] R. Ding and N. Bowler, "Permittivity and electrical breakdown response of nylon 6 to chemical exposure," *IEEE Transactions on Dielectrics and Electrical Insulation*, pp. 1151–1160, 2015.

[62] M. Ieda, "Dielectric breakdown process of polymers," *IEEE Transactions on Electrical Insulation*, no. 3, pp. 206–224, 1980.

[63] M. M. Gauthier, *Engineered materials handbook*. Materials Park, OH 44073-0002, USA: ASM International, 1995.

[64] "ASTM d257 - 14(2021)e1: Standard test methods for dc resistance or conductance of insulating materials," ASTM International, West Conshohocken, PA, Standard, 2021.

[65] S. Singh, M. Mohsin, and A. Masood, "Prediction of breakdown strength of cellulosic insulating materials using artificial neural networks," *Journal of Advanced Dielectrics*, p. 1 850 003, 2018.

[66] Www.goodfellow.com, *Polyhydroxybutyrate - biopolymer (PHB)*. [Online]. Available: `http://www.goodfellow.com/A/Polyhydroxybutyrate-Biopolymer.html` (visited on 12/20/2021).

[67] *Polymer - electrical properties*. [Online]. Available: `http://www.goodfellow.com/catalogue/GFCat2C.php?ewd_token=qetccDHivUVzGlnWYJE7sWnZ1AqjTD&n=V2sF6eWbanssnixAPysNFQHwOnH83V&ewd_urlNo=GFCat26&type=30&prop=5` (visited on 12/20/2021).

[68] ——, *Cellulose acetate (CA)*. [Online]. Available: `http://www.goodfellow.com/A/Cellulose-Acetate-Polymer.html` (visited on 12/20/2021).

[69] A. Luckow, M. Santcroos, O. Weidner, A. Merzky, S. Maddineni, and S. Jha, *Proceedings of the 21st international symposium on high-performance parallel and distributed computing, HPDC'12*, 2012.

[70] A. Rakowska and K. Hajdrowski, "Influence of different test conditions on volume resistivity of polymeric insulated cables and polyethylene samples," in *2000 Eighth International Conference on Dielectric Materials, Measurements and Applications (IEE Conf. Publ. No. 473)*, 2000, pp. 281–284. DOI: `10.1049/cp:20000519`.

[71] A. Bhowmick, *Rubber products manufacturing technology*. Oxfordshire, England, UK: Routledge, 2018, p. 677.

[72] A. Peacock, *Handbook of polyethylene: structures: properties, and applications*. Boca Raton, Florida, USA: CRC press, 2000, pp. 123–241.

[73] H. Yazdani, B. E. Smith, and K. Hatami, "Electrical conductivity and mechanical performance of multiwalled cnt-filled polyvinyl chloride composites subjected to tensile load," *Journal of Applied Polymer Science*, 2016.

[74] H. E. Yang, R. French, and L. Bruckman, *Durability and Reliability of Polymers and Other Materials in Photovoltaic Modules*. William Andrew, 2019.

[75] *Material properties and specification of nylon 6*, Ai Engineering Plastics Laminates, 2017. [Online]. Available: `https://www.aiplastics.com/media/amari/datasheets/Nylon-6%20Datasheet.pdf` (visited on 12/20/2021).

[76] H. Gharanjig, K. Gharanjig, M. Hosseinnezhad, and S. M. Jafari, "Differential scanning calorimetry (dsc) of nanoencapsulated food ingredients," in *Characterization of Nanoencapsulated Food Ingredients*, Elsevier, 2020, pp. 295–346.

[77] "ASTM d3418–03 : Standard test method for transition temperatures of polymers by differential scanning calorimetry," ASTM International, West Conshohocken, PA, Standard, 1999.

[78] J. Abraham, A. P. Mohammed, M. A. Kumar, S. C. George, and S. Thomas, "Thermoanalytical techniques of nanomaterials," in *Characterization of Nanomaterials*, Elsevier, 2018, pp. 213–236.

[79] M. P. Sepe, *Thermal analysis of polymers*. Shropshire, SY4 4NR, United Kingdom: Rapra Technology Limited, 1997, pp. 3–5.

[80] A. Shrivastava, *Introduction to plastics engineering*. William Andrew, 2018, pp. 1–16.

[81] E. Rudnik, *Compostable polymer materials*. Amsterdam, The Netherlands: Elsevier Science, 2019, pp. 50–92.

[82] G. Pratt and H. Smith, "Dielectric spectroscopy of some" biopol" polymers," in *Proceedings of 1995 IEEE 5th International Conference on Conduction and Breakdown in Solid Dielectrics*, IEEE, 1995, pp. 28–32.

[83] S. El-Taweel, G. Höhne, A. Mansour, B. Stoll, and H. Seliger, "Glass transition and the rigid amorphous phase in semicrystalline blends of bacterial polyhydroxybutyrate phb with low molecular mass atactic r, s-phb-diol," *Polymer*, pp. 983–992, 2004.

[84] J. P. Mofokeng and A. S. Luyt, "Dynamic mechanical properties of PLA/PHBV, PLA/PCL, PHBV/PCL blends and their nanocomposites with TiO2 as nanofiller," *Thermochimica Acta*, vol. 613, pp. 41–53, 2015.

[85] M. A. Woodruff and D. W. Hutmacher, "The return of a forgotten polymer—polycaprolactone in the 21st century," *Progress in polymer science*, pp. 1217–1256, 2010.

[86] S. Lampman *et al.*, *Characterization and failure analysis of plastics*. Materials Park, OH 44073-0002, USA.: ASM International, 2003, pp. 116–118.

[87] R. Homklin and N. Hongsriphan, "Mechanical and thermal properties of PLA/PBS co-continuous blends adding nucleating agent," *Energy Procedia*, vol. 34, pp. 871–879, 2013.

[88] M. L. Di Lorenzo, R. Androsch, and M. C. Righetti, "Low-temperature crystallization of poly (butylene succinate)," *European Polymer Journal*, pp. 384–391, 2017.

[89] L. Jiang, M. P. Wolcott, and J. Zhang, "Study of biodegradable polylactide/poly (butylene adipate-co-terephthalate) blends," *Biomacromolecules*, pp. 199–207, 2006.

[90] S. Mohanty and S. Nayak, "Biodegradable nanocomposites of poly (butylene adipate-co-terephthalate)(pbat) and organically modified layered silicates," *Journal of Polymers and the Environment*, pp. 195–207, 2012.

[91] K. Kamide and M. Saito, "Thermal analysis of cellulose acetate solids with total degrees of substitution of 0.49, 1.75, 2.46, and 2.92," *Polymer Journal*, pp. 919–928, 1985.

[92] L. Boukezzi, A. Boubakeur, C. Laurent, and M. Lallouani, "DSC study of artificial thermal aging of XLPE insulation cables," in *2007 IEEE International Conference on Solid Dielectrics*, IEEE, 2007, pp. 146–149.

[93] A. M. de Andrade, R. Faria, F. J. Fonseca, E. Dirani, W. Pinheiro, and J. Oliveira, "Tsc and dsc measurements of polymeric insulators used in medium voltage distribution cables," in *Proceedings of 8th International Symposium on Electrets (ISE 8)*, IEEE, 1994, pp. 911–915.

[94] F. Li, W. Zhu, X. Zhang, C. Zhao, and M. Xu, "Shape memory effect of ethylene–vinyl acetate copolymers," *Journal of Applied Polymer Science*, pp. 1063–1070, 1999.

[95] "ASTM d638-14, standard test method for tensile properties of plastics," ASTM International, West Conshohocken, PA, Standard, 2015.

[96] "ASTM d882-10, standard test method for tensile properties of thin plastic sheeting," ASTM International, West Conshohocken, PA, Standard, 2010.

[97] "ASTM d6287-17, standard practice for cutting film and sheeting test specimens," ASTM International, West Conshohocken, PA, Standard, 2017.

[98] I. P. Herman, "Mechanical properties of the body," in *Physics of the Human Body*, Springer, 2016, pp. 247–329.

[99] Y. Liu, O. Stein, J. H. Campbell, L. Jiang, N. Petta, and Y. Lu, "Three-dimensional printing and deformation behavior of low-density target structures by two-photon polymerization," in *Nanoengineering: Fabrication, Properties, Optics, and Devices XIV*, International Society for Optics and Photonics, vol. 10354, 2017, p. 103 541.

[100] G. M. Swallowe, *Mechanical Properties and Testing of Polymers: an A–Z reference*. Springer Science & Business Media, 1999, vol. 3.

[101] M. Koenig and S. Huang, "Biodegradable blends and composites of polycaprolactone and starch derivatives," *Polymer*, pp. 1877–1882, 1995.

[102] P. Matzinos, V. Tserki, A. Kontoyiannis, and C. Panayiotou, "Processing and characterization of starch/polycaprolactone products," *Polymer Degradation and Stability*, pp. 17–24, 2002.

[103] S. Eshraghi and S. Das, "Mechanical and microstructural properties of polycaprolactone scaffolds with 1-d, 2-d, and 3-d orthogonally oriented porous architectures produced by selective laser sintering," *Acta biomaterialia*, p. 2467, 2010.

[104] T. Uesaka, K. Nakane, S. Maeda, T. Ogihara, and N. Ogata, "Structure and physical properties of poly (butylene succinate)/cellulose acetate blends," *Polymer*, pp. 8449–8454, 2000.

[105] Z.-Y. Yang, W.-J. Wang, Z.-Q. Shao, H.-D. Zhu, Y.-H. Li, and F.-J. Wang, "The transparency and mechanical properties of cellulose acetate nanocomposites using cellulose nanowhiskers as fillers," *Cellulose*, pp. 159–168, 2013.

[106] A. C. Wibowo, M. Misra, H.-M. Park, L. T. Drzal, R. Schalek, and A. K. Mohanty, "Biodegradable nanocomposites from cellulose acetate: Mechanical, morphological, and thermal properties," *Composites Part A: Applied Science and Manufacturing*, pp. 1428–1433, 2006.

[107] P. Visakh and S. Lüftl, *Polyethylene-based biocomposites and bionanocomposites*. Hoboken, NJ 07030, USA.: John Wiley & Sons, 2016.

[108] Y. Mecheri, L. Boukezzi, A. Boubakeur, and M. Lallouani, "Dielectric and mechanical behavior of cross-linked polyethylene under thermal aging," in *2000 Annual report conference on electrical insulation and dielectric phenomena (Cat. No. 00CH37132)*, IEEE, 2000, pp. 560–563.

[109] J.-H. Lee, K. S. Suh, S.-J. Kim, D.-W. Jeong, and M.-K. Han, "Water tree retardation and electrical properties of eva blended xlpe," in *[1992] Proceedings of the 4th International Conference on Conduction and Breakdown in Solid Dielectrics*, IEEE, 1992, pp. 451–455.

[110] M. Alexandre, G. Beyer, C. Henrist, R. Cloots, A. Rulmont, R. Jérôme, and P. Dubois, "Preparation and properties of layered silicate nanocomposites based on ethylene vinyl acetate copolymers," *Macromolecular rapid communications*, pp. 643–646, 2001.

[111] "ASTM d1816-12(2019): Standard test method for dielectric breakdown voltage of insulating liquids using VDE electrodes," ASTM International, West Conshohocken, PA, Standard, 2019.

[112] I. E. Commission *et al.*, "IEC 62631-3-1: 2016 dielectric and resistive properties of solid insulating materials—part 3-1: Determination of resistive properties (dc methods)—volume resistance and volume resistivity—general method," *International Electrotechnical Commission: Geneva, Switzerland*, 2016.

[113] S. Li, Y. Zhu, D. Min, and G. Chen, "Space charge modulated electrical breakdown," *Scientific reports*, pp. 1–4, 2016.

[114] J. Hayden and W. Eddy, "Dielectric strength ratio between alternating and direct voltages," *Journal of the American Institute of Electrical Engineers*, pp. 706–712, 1923.

[115] D. Robinson, "The breakdown mechanism of impregnated paper cables," *Journal of the Institution of Electrical Engineers*, pp. 90–103, 1935.

[116] J. Seong, I. Seo, J. Hwang, and B. Lee, "Comparative evaluation between DC and AC breakdown characteristic of dielectric insulating materials in liquid nitrogen," *IEEE transactions on applied superconductivity*, 2011.

[117] M. Balpinarli, J. Dai, and G. Gela, "AC and DC breakdown versus thickness characteristics for rubber gloves," *IEEE transactions on power delivery*, pp. 384–391, 1988.

[118] T. Jow and P. Cygan, "Investigation of dielectric breakdown of polyvinylidene fluoride using ac and dc methods," in *Conference Record of the 1992 IEEE International Symposium on Electrical Insulation*, IEEE, 1992, pp. 181–184.

[119] S. Banerjee, "A study of high frequency voltage effects in medium voltage cable terminations," M.S. thesis, University of Waterloo, 2008.

[120] J. C. C. Yeo, J. K. Muiruri, W. Thitsartarn, Z. Li, and C. He, "Recent advances in the development of biodegradable phb-based toughening materials: Approaches, advantages and applications," *Materials Science and Engineering: C*, vol. 92, pp. 1092–1116, 2018.

[121] W. Dong, P. Ma, S. Wang, M. Chen, X. Cai, and Y. Zhang, "Effect of partial crosslinking on morphology and properties of the poly (β-hydroxybutyrate)/poly (d, l-lactic acid) blends," *Polymer degradation and stability*, vol. 98, no. 9, pp. 1549–1555, 2013.

[122] F. M. Kapritchkoff, A. P. Viotti, R. C. Alli, M. Zuccolo, J. G. Pradella, A. E. Maiorano, E. A. Miranda, and A. Bonomi, "Enzymatic recovery and purification of polyhydroxybutyrate produced by ralstonia eutropha," *Journal of biotechnology*, vol. 122, no. 4, pp. 453–462, 2006.

[123] B. Wang, R. R. Sharma-Shivappa, J. W. Olson, and S. A. Khan, "Production of polyhydroxybutyrate (phb) by alcaligenes latus using sugarbeet juice," *Industrial crops and products*, vol. 43, pp. 802–811, 2013.

[124] A. Garcıa, D. Segura, G. Espın, E. Galindo, T. Castillo, and C. Peña, "High production of poly-β-hydroxybutyrate (phb) by an azotobacter vinelandii mutant altered in phb regulation using a fed-batch fermentation process," *Biochemical engineering journal*, vol. 82, pp. 117–123, 2014.

[125] P. Singh and N. Parmar, "Isolation and characterization of two novel polyhydroxybutyrate (phb)-producing bacteria," *African journal of biotechnology*, vol. 10, no. 24, pp. 4907–4919, 2011.

[126] S. W. Kim, P. Kim, H. S. Lee, and J. H. Kim, "High production of poly-β-hydroxybutyrate (phb) from methylobacterium organophilum under potassium limitation," *Biotechnology letters*, vol. 18, no. 1, pp. 25–30, 1996.

[127] T. G. Volova, *Polyhydroxyalkanoates–plastic materials of the 21st century: production, properties, applications*. Nova publishers, 2004.

[128] R. Britton, *Update on Mouldable Particle Foam Technology*. iSmithers, 2009, p. 97, ISBN: 978-1-84735-406-8.

[129] C. Reddy, R. Ghai, V. Kalia, *et al.*, "Polyhydroxyalkanoates: An overview," *Bioresource technology*, vol. 87, no. 2, pp. 137–146, 2003.

[130] M. L. Tebaldi, A. L. C. Maia, F. Poletto, F. V. de Andrade, and D. C. F. Soares, "Poly (-3-hydroxybutyrate-co-3-hydroxyvalerate)(PHBV): Current advances in synthesis methodologies, antitumor applications and biocompatibility," *Journal of Drug Delivery Science and Technology*, pp. 115–126, 2019.

[131] M. I. Ibrahim, D. Alsafadi, K. A. Alamry, and M. A. Hussein, "Properties and applications of poly (3-hydroxybutyrate-co-3-hydroxyvalerate) biocomposites," *Journal of Polymers and the Environment*, pp. 1010–1030, 2021.

[132] S. Modi, K. Koelling, and Y. Vodovotz, "Assessment of PHB with varying hydroxyvalerate content for potential packaging applications," *European Polymer Journal*, pp. 179–186, 2011.

[133] E. Castro-Aguirre, F. Iniguez-Franco, H. Samsudin, X. Fang, and R. Auras, "Poly (lactic acid)—mass production, processing, industrial applications, and end of life," *Advanced drug delivery reviews*, vol. 107, pp. 333–366, 2016.

[134] C. V. Stevens, *Bio-based plastics: materials and applications*. West Sussex, United Kingdom: John Wiley & Sons, 2013, pp. 35–59.

[135] M. Labet and W. Thielemans, "Synthesis of polycaprolactone: A review," *Chemical society reviews*, vol. 38, no. 12, pp. 3484–3504, 2009.

[136] Y. Ikada and H. Tsuji, "Biodegradable polyesters for medical and ecological applications," *Macromolecular rapid communications*, vol. 21, no. 3, pp. 117–132, 2000.

[137] F. V. Ferreira, L. S. Cividanes, R. F. Gouveia, and L. M. Lona, "An overview on properties and applications of poly (butylene adipate-co-terephthalate)–pbat based composites," *Polymer Engineering & Science*, vol. 59, no. s2, E7–E15, 2019.

[138] J. Jian, Z. Xiangbin, and H. Xianbo, "An overview on synthesis, properties and applications of poly (butylene-adipate-co-terephthalate)–pbat," *Advanced Industrial and Engineering Polymer Research*, vol. 3, no. 1, pp. 19–26, 2020.

[139] J. Xu and B.-H. Guo, "Poly (butylene succinate) and its copolymers: Research, development and industrialization," *Biotechnology journal*, vol. 5, no. 11, pp. 1149–1163, 2010.

[140] Y.-J. Wee, J.-S. Yun, K.-H. Kang, and H.-W. Ryu, "Continuous production of succinic acid by a fumarate-reducing bacterium immobilized in a hollow-fiber bioreactor," in *Biotechnology for Fuels and Chemicals*, Springer, 2002, pp. 1093–1104.

[141] D. B. Malpass, *Introduction to industrial polyethylene: properties, catalysts, and processes*. Hoboken, New Jersey, USA: John Wiley & Sons, 2010, pp. 23–29.

[142] S. Saurav, "XLPE manufacturing processes," in *Crosslinkable Polyethylene: Manufacture, Properties, Recycling, and Applications*, Gateway East, Singapore 189721, Singapore.: Springer Nature, 2021, pp. 41–61.

[143] R. P. d. Melo, V. d. O. Aguiar, and M. d. F. V. Marques, "Silane crosslinked polyethylene from different commercial pe's: Influence of comonomer, catalyst type and evaluation of hlpb as crosslinking coagent," *Materials Research*, vol. 18, pp. 313–319, 2015.

[144] S. Patrick, *PVC compounds and processing*. Shrewsbury, Shropshire, United Kingdom: Rapra Technology, 2004, vol. 15, p. 4.

[145] G. Marianne and P. Stuart, "Poly(vinyl chloride)," in *Brydson's Plastics Materials*, G. Marianne, Ed., Cambridge, MA 02139, USA: Elsevier, 2017, pp. 329–388.

[146] R. Wheeler Jr, "Poly (vinyl chloride) processes and products.," *Environmental health perspectives*, vol. 41, pp. 123–128, 1981.

[147] M. Mishra and Y. Yagci, "Polyvinyl acetate," in *Handbook of vinyl polymers: radical polymerization, process, and technology*, Boca Raton, FL 33487-2742, USA: CRC Press, 2016, pp. 413–418.

[148] J. K. Fink, *Handbook of engineering and speciality thermoplastics: Polyolefins and Styrenics*. Beverly, MA 01915, USA: Scrivener Publ., 2011, p. 187.

[149] X. Fang, C. D. Simone, E. Vaccaro, S. J. Huang, and D. A. Scola, "Ring-opening polymerization of -caprolactam and -caprolactone via microwave irradiation," *Journal of Polymer Science Part A: Polymer Chemistry*, vol. 40, no. 14, pp. 2264–2275, 2002.

[150] J. Thomas, *Crosslinkable Polyethylene: Manufacture, Properties, Recycling, and Applications*. Gateway East, Singapore 189721, Singapore.: Springer Nature, 2021.

[151] G. G. Raju, *Dielectrics in electric fields: Tables, Atoms, and Molecules*. Boca Raton, FL 33487-2742, USA: CRC press, 2017.

Appendix A

List of materials investigated

A.1 Bio-polymeric materials studied

A.1.1 Polyhydroxybutyrate (PHB) and Poly(3 - hydroxybutyrate - co - 3 - hydroxyvalerate) (PHBV)

Polyhydroxybutyrate (PHB) is a bio-polymer generated using microorganisms, such as *Ralstonia eutropha* [122], *Alcaligenes latus* [123], *Azotobacter vinelandii* [124], *Pseudomonas olevorans* [125], *Methylobacterium organophilum* [126] etc. Selected bacteria is placed in bio substrate and provided high level of nutrients for reproduction, when an considerable population generated, bacteria are deprived of nutrients such as nitrogen, oxygen and phosphorus and fed high levels of carbon. Then bacteria reserves/stores carbon in the form of PHB in their granules until other nutrients are available. Generated PHB is harvested by drying the bacteria in a controlled environment and then subjected to a number of refining processes. Resulting polymer is biodegradable and safe for contact with living tissue, thus often used in medical applications. With good barrier properties and bio-degradability it is used for single-use food packaging as well [127]. PHB falls under the family of polyhydroxyalkanoates (PHA) as illustrated in Figure A.4. There are several types of PHB polymers and co-polymers formed during the enzymatic digestion process [128].

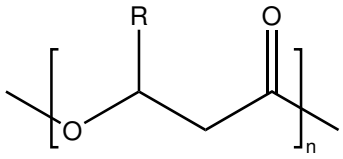

Figure A.1. *Chemical structure of polyhydroxyalkanoate (PHA) produced in bacteria [129].*

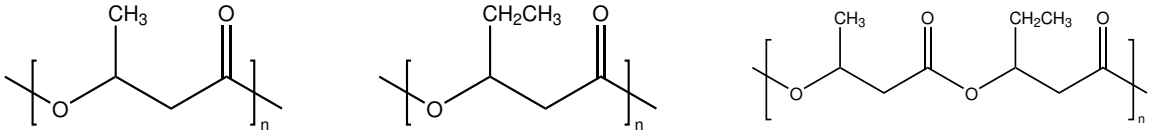

(a) *PHB* ***(b)*** *PHV* ***(c)*** *PHBV*

Figure A.2. *Chemical structures of polyhydroxybutyrate (PHB), polyhydroxyvalerate (PHV) and poly(3-hydroxybutyrate-co-3-hydroxyvalerate)copolymer (PHBV)*

Poly(3-hydroxybutyrate-co3-hydroxyvalerate) (PHBV) is a co-polymer created from the combination of polyhydroxybutyrate (PHB) and polyhydroxyvalerate (PHV). Compared to other PHAs, PHBV is gaining more and more attention in biomedical applications [130]. This is mainly due to its improved flexibility, biodegradability and compatibility with human tissue [131]. Compared to PHB, PHBV is flexible and has lower melting and glass transition temperatures, therefore has a wider processing window [132].

A.1.2 Polylactic acid (PLA)

More often polylactic acid (PLA) is generated from sugarcane and corn starch sources. First lactic acid (LA) is produced by bacterial fermentation. Two stereo isomers are generated as a results, specifically L-LA and D-LA. There are two methods to produce high molecular weight (mw $>$ 100kDpa) PLA from these monomers, namely poly-condensation and ring-opening polymerization [133].

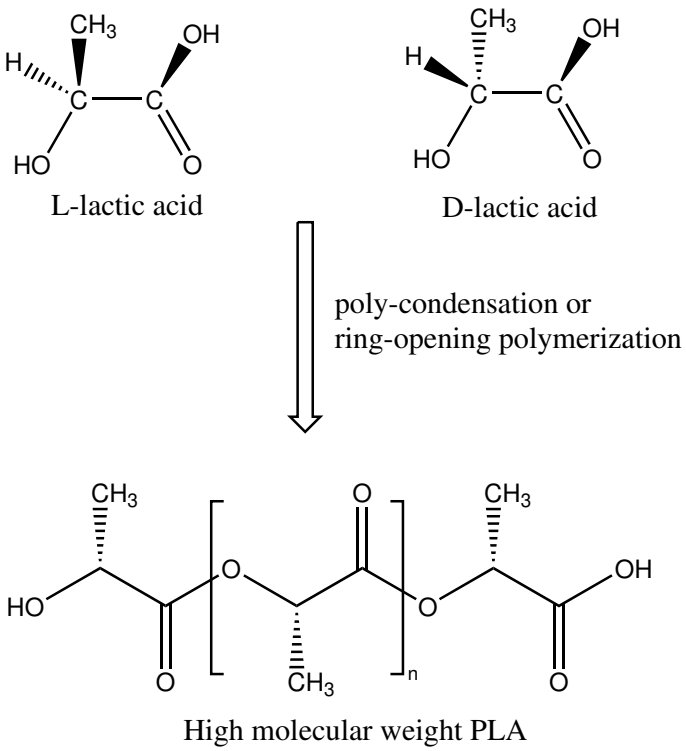

Figure A.3. *Chemical process of generating polylactic acid (PLA) from lactic acid (LA).*

At present PLA can be industrially processed by injection molding, thin film extrusion, fiber spinning and thermoforming. Commercially, PLA is used to manufacture food packaging, medical devices and 3D printing filament etc. PLA degrades by the hydrolysis of the ester bond and does not require enzymatic digestion.

A.1.3 Cellulose acetate (CA)

Cellulose acetate is a biodegradable polymer generated by esterification of cellulose. Cellulose acetate was discovered in 1865 making it one of the oldest synthetic polymers. In-order to produce cellulose acetate first cellulose fibers are extracted from wood, paper and biomass and purified into pulp. Then it is reacted with acetic acid and acetic anhydride in the presence of sulfuric acid. It is available in the form of

fibers and sheet. Biggest disadvantage of cellulose acetate is its reactivity to acids and alkali solutions [134].

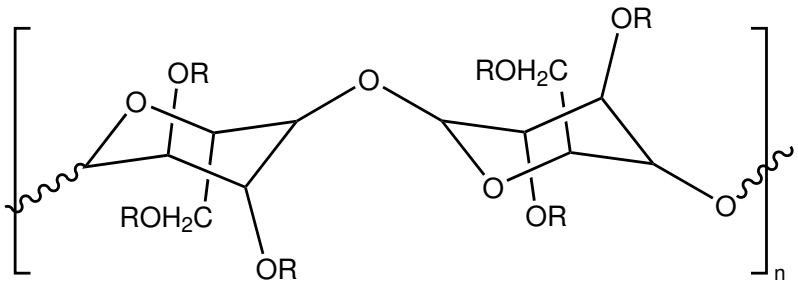

Figure A.4. *Chemical structure of cellulose acetate (CA)*

A.1.4 Polycaprolactone (PCL)

Polycaprolactone (PCL) is an important polymer when it comes to miscibility with other polymers. It can be combined with polymers such as poly vinyl chloride (PVC), poly styrene acrylonitrile copolymer, poly acrylonitrile-butadiene-styrene (ABS), polycarbonates, nitrocellulose and cellulose butyrate etc. PCL biodegrades under natural microbial digestion in the environment[135]. However this degradation is minimal under enzymatic conditions inside the human body [136]. Therefore, PCL is used in biomedical applications such as medical implants etc.

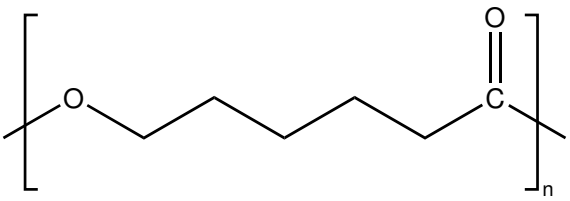

Figure A.5. *Chemical structure of polycaprolactone (PCL)*

A.1.5 Polybutyleneadipate-co-terephthalate (PBAT)

Polybutyleneadipate-co-terephthalate (PBAT) is a synthetic biodegradable polymer. It can be generated by polycondensation of butanediol (BDO), adipic acid (AA) and terephthalic acid (PTA). PBAT is also used in biomedical applications, food packaging and in agricultural products [137]. PBAT is biodegradable in natural compost environment at elevated temperatures around 60 ^{0}C [138].

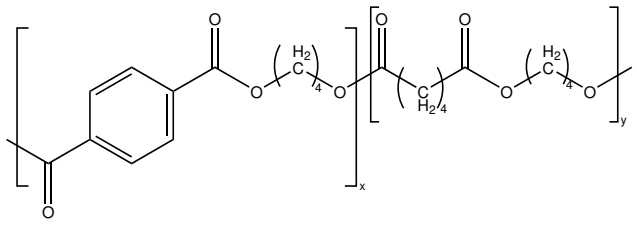

Figure A.6. *Chemical structure of Polybutyleneadipate-co-terephthalate (PBAT)*

A.1.6 Poly butylene succinate (PBS)

Poly butylene succinate (PBS) is a biodegradable polymer made from mainly fossil fuel based sources. The commercial source of manufacturing PBS is from 1,4-butanediol (BDO) extracted from a petrochemical feed-stock. Then succinic acid and BDO are processed through esterification to obtain oligomers. Next step is ploycondensation which result in high molecular weight PBS [139]. PBS can also synthesised from fermentation of microorganisms on a bio-based feed stock [140]. However, commercially conventional fossil fuel based manufacturing process is still dominant due to the low manufacturing cost. PBS is mainly used to produce agricultural mulching films, compostable bags and single use food utensils.

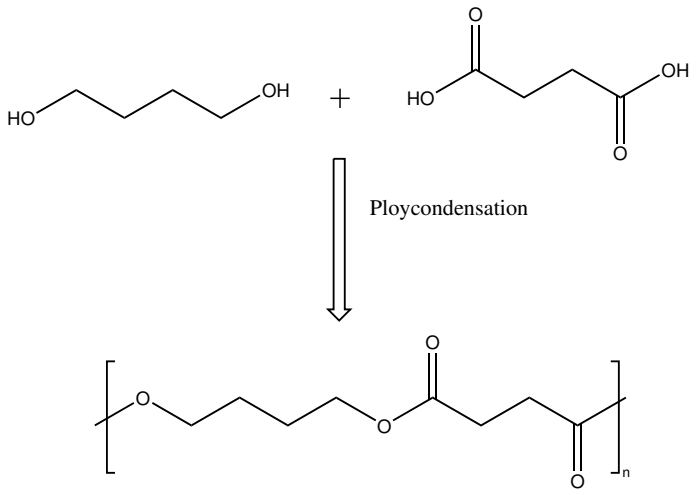

Figure A.7. *Chemical structure of Poly butylene succinate (PBS)*

A.2 Fossil fuel based polymeric materials studied

A.2.1 Low density polyethylene (LDPE)

Polyethylene or LDPE is the most widely consumed polymer currently in the world. The uses of LDPE range from packaging, piping, machine parts, electrical insulation etc. Polyethylene is manufactured by polymerisation of monomer ethylene as illustrated by figure A.8. Ethylene is a produced mainly during fossil fuel cracking in oil refining plants. Cracking is the process of breaking down complex hydrocarbons present in fossil fuel into smaller components for commercial use, such as gasoline and diesel. Ethylene can be generated by other means such as dehydration of ethanol, but the conventional fossil fuel based generation strategy is dominant due to low cost of production. Main polymerization methods used in industry to convert ethylene into polyethylene are slurry, solution, high pressure autoclave, high pressure tubular and gas-phase process [141].

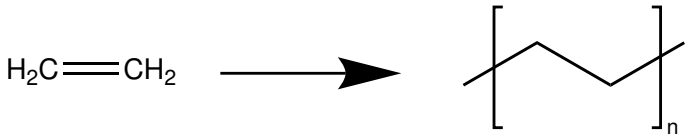

Figure A.8. *Chemical reaction for commercial production of of Polyethylene*

A.2.2 Cross linked polyethylene (XLPE)

XLPE is manufactured through cross-linking of LDPE. Cross-linking is the process of combining two separate polymer chain molecules to form a single molecule. Corss-linking limit chain movement and improve the molecular density. There three main cross-linking methods when it comes to manufacturing XLPE, radiation cross-linking, peroxide cross-linking and silane cross-linking [142].

In radiation cross-linking LDPE feed-stock is subjected to a high energy electron beam. The electron beam excite the LDPE molecules to a super-excited state. In this excited state molecules are decomposed into free radicals causing a large number of free radical cross-linking reactions. Cross-linking efficiency is improved by increasing the pressure [142]. In peroxide cross-linking as the first step, organic peroxides such as dicumyl peroxide (DCP) are melt blended with LDPE. Free radicals are released from peroxides through thermolytic decomposition. These free radicals react with linear polymer chains to form a network of cross-links. Primary reaction involved in cross-linking is shown in figure A.9, however there is a large number of secondary reactions involved depending on the reaction conditions [143]. Silane cross-linking is different than the two methods discussed earlier. Here vinyltriethoxysilane (VTES) or vinyltrimethoxysilane (VTMS) is grafted in LDPE with a small quantity of peroxide initiators. Then mixture is subjected to hydrolysis and condensation. Unlike radiation and peroxide cross-linking, the cross-linking bond is created between the silanol groups, as illustrated in figure A.10.

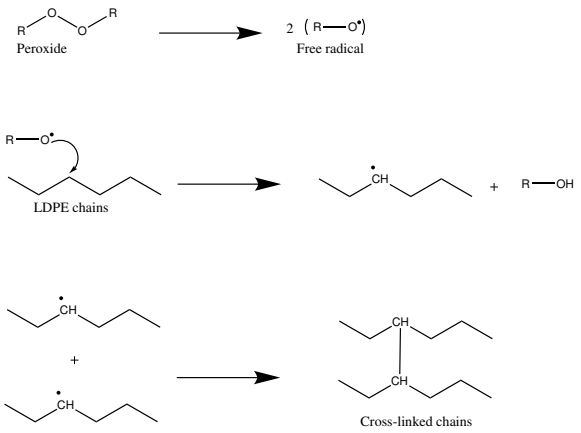

Figure A.9. *Main reaction of peroxide cross-linking for XLPE manufacturing [143]*

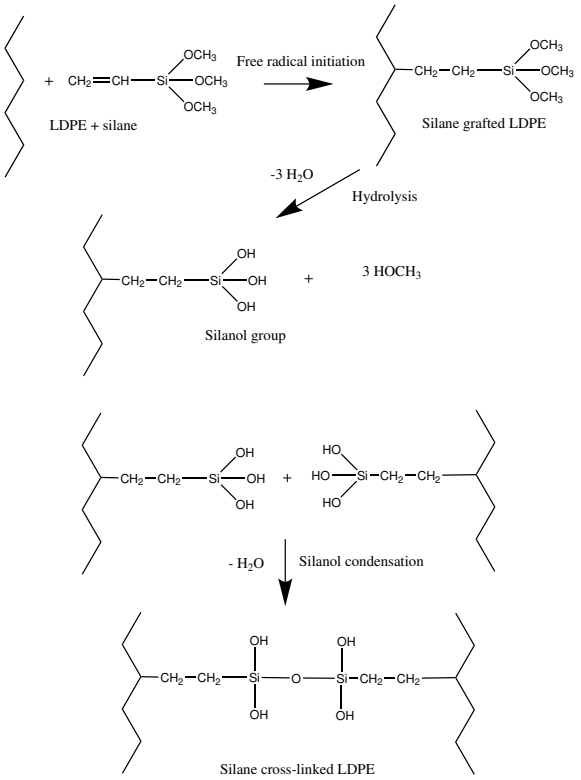

Figure A.10. *Main reaction of silane cross-linking for XLPE manufacturing [143]*

A.2.3 Poly vinyl chloride (PVC)

Poly vinyl chloride (PVC) is manufactured through polymerization of vinyl chloride monomer (VCM). VCM is commercially produced by reacting ethylene and chlorine as illustrated in figure A.11 [144]. There are four main processes for industrial man-

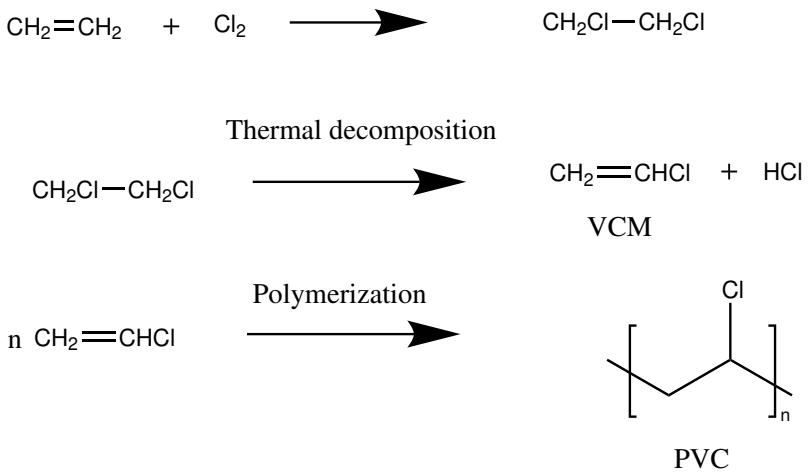

Figure A.11. *Chemical reactions for commercial production of PVC.*

ufacturing of PVC from VCM, specifically, suspension, bulk, emulsion and solution processes. Suspension polymerisation is carried out in an pressurized autoclave reactor. Raw materials vinyl chloride monomer (VCM) is pressurized and liquefied and fed into the reactor along with water. Small droplets of VCM are formed inside the autoclave due to vigorous agitation. Polymerization occurs when peroxide initiators are fed into the reactor at this conditions. Resulting polyvinyl chloride particles are collected as a slurry from the bottom of the reactor. This slurry is purified and PVC is extracted as a powder form. However, PVC particles produced by this method has a skin around them formed by suspending residues. Bulk polymerization produces PVC particles without this skin. VCM and free radical initiator are vigorously agitated (without any water) together in the initial polymerization stage. However, unlike in suspension polymerization, formed PVC particles absorb unreacted monomer and

the viscosity increases as the PVC particles are formed. Then salary is transferred to a second reactor and additional VCM is added upto a conversion rate of 80-85 % is achieved. Resulting slurry is purified to obtain PVC in particle form. In emulsion polymerization, instead of water polymerization occurs in a emulsion. Common emulsions used are alkali salts and alkyl sulfates. Rapid polymerization is expected in a emulsion when compared to water. Other conversion steps are similar to suspension polymerization [145]. Solution polymerization is different to the methods discussed earlier. Here, vinyl chloride monomer, co-monomer, solvent and initiator are fed into a continues reactor system. Generated PVC dissolves in the solvent and a viscus slurry is produced. This slurry is purified and often used as a coating material [146].

A.2.4 Ethylene vinyl acetate (EVA)

Ethylene vinyl acetate is produced by polymerizing ethylene and vinyl acetate. Ethylene is produced as a byproduct of fossil-fuel cracking as discussed earlier. Vinyl acetate is produced by oxidation of ethylene and acetic acid. Ethylene and vinyl acetate are liquefied and polymerized in a reactor. Similar to PVC, suspension, mass, emulsion and solution polymerization are the main industrial processes to manufacture EVA. [147], [148].

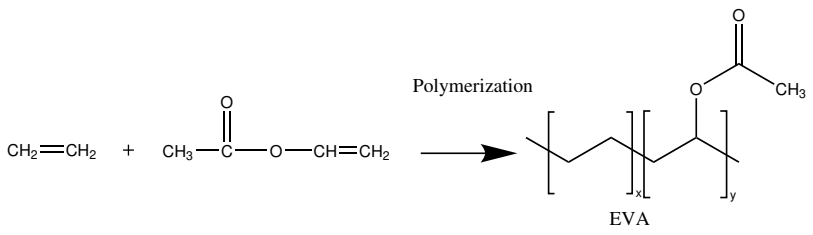

Figure A.12. *Chemical reactions for commercial production of EVA.*

A.2.5 Polycaprolactam (NYLON 6)

NYLON 6 is commercially produced by ring opening polymerization of ϵ-caprolactam as illustrated in figure A.13. Ring opening of ϵ-caprolactam occurs at a temperature range of 250-270 ^0C in a high-pressure reactor using 5-10 % of water and a initiator. When the polymer-chains grow, the viscosity of the solution increases and NYLON-6 is extracted in the molten form. Then molten NYLON-6 is water cooled and palatalized [149].

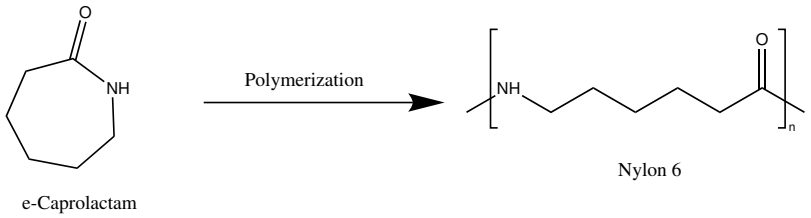

Figure A.13. *Chemical reactions for commercial production of NYLON 6.*

Appendix B

Results of dielectric measurements

B.1 Real and imaginary dielectric constant

Dielectric properties for frequency range of 1-10^5 Hz was measured using Solartron Modulab dielectric spectroscope. Thickness was measured using the inbuilt micrometer assembly of the sample holder. 5 thickness readings were taken and averaged to obtain the thickness reported in table B.1. Measurements of real relative permittivity and imaginary relative permittivity were obtained for the mentioned frequency range. Average values or real and imaginary relative permittivity for each sample were reported in table B.1. All measurements were taken in room temperature measured 22 ^0C. As mentioned in section 3.1, sample names specifies the chemical name, weight concentration of the solution and the rotational speed used in sample preparation.

Table B.1. *Real and imaginary relative permittivity of samples.*

Sample name	**Thickness**	**Real**	**Imaginary**
	mm	$\epsilon_r^{'}$	$\epsilon_r^{''}$
PHB(10)-500-1	0.029 ± 0.003	2.18	0.019
PHB(10)-500-2	0.029 ± 0.002	2.38	0.021
PHB(10)-500-3	0.029 ± 0.002	2.29	0.020
PHB(10)-500-4	0.026 ± 0.004	2.4	0.021

Continued on next page

Table B.1 – *Continued from previous page*

Sample name	**Thickness**	**Real**	**Imaginary**
PHB/PHV[80:20](20)-500-1	0.030 ± 0.002	3.66	0.020
PHB/PHV[80:20](20)-500-2	0.029 ± 0.002	3.21	0.035
PHB/PHV[80:20](20)-500-3	N/A	N/A	N/A
PHB/PHV[80:20](20)-500-4	0.029 ± 0.001	3.34	0.026
PHB/PHV[80:20](20)-500-5	0.025 ± 0.002	3.10	0.028
PCL(20)-1000-1	0.022 ± 0.003	3.51	0.039
PCL(20)-1000-2	0.015 ± 0.001	3.25	0.044
PCL(20)-1000-3	0.018 ± 0.002	2.98	0.025
PCL(20)-1000-4	0.020 ± 0.001	2.98	0.028
PBS(20)-750-1	0.025 ± 0.002	4.59	0.052
PBS(20)-750-2	0.024 ± 0.003	4.91	0.067
PBS(20)-750-3	0.022 ± 0.003	4.58	0.018
PBAT(25)-750-1	0.029 ± 0.002	4.67	0.031
PBAT(25)-750-2	0.029 ± 0.001	4.84	0.037
PBAT(25)-750-3	0.026 ± 0.002	4.77	0.031
PBAT(25)-750-4	0.029 ± 0.002	4.87	0.046
PLA(10)-750-1	0.021 ± 0.002	2.61	0.020
PLA(10)-750-2	0.022 ± 0.002	2.80	0.009
PLA(10)-750-3	0.020 ± 0.002	2.17	0.010
PLA(10)-750-4	0.020 ± 0.001	2.19	0.009

B.2 Dielectric breakdown strength

Table B.2 report average of dielectric breakdown measurements done on each sample. Thickness is averaged from 5 measurements and breakdown voltage is averaged from 4 measurements for each sample. Measurements were done in room temperature measured 22 ^0C. Air breakdown voltage for a electrode gap of 0.051mm was measured 541V, whereas the air breakdown strength was calculated 10.6 kV/mm.

Table B.2. *Dielectric breakdown strength, average breakdown voltage and average thickness of measured samples.*

Sample name	**Thickness**	**Breakdown voltage**	**DBS**
	mm	**kV**	**kV/mm**
PHB(15)-750-1	0.025 ± 0.003	1.553	30.4
PHB(15)-750-2	0.024 ± 0.003	1.488	29.2
PHB(15)-750-3	0.025 ± 0.003	1.423	27.9
PHB/PHV[88:12](20)-500-1	0.021 ± 0.001	0.575	11.3
PHB/PHV[88:12](20)-500-2	0.023 ± 0.003	0.593	11.6
PHB/PHV[88:12](20)-500-3	0.021 ± 0.002	0.573	11.2
PCL(12)-500-1	0.026 ± 0.003	0.837	16.4
PCL(12)-500-2	0.025 ± 0.003	0.864	16.9
PCL(12)-500-3	0.026 ± 0.002	0.999	19.6
PBS(20)-500-1	0.023 ± 0.002	0.801	15.7
PBS(20)-500-2	0.023 ± 0.002	0.747	14.6
PBS(20)-500-3	0.022 ± 0.002	0.810	15.8
PBAT(20)-500-1	0.022 ± 0.003	1.553	30.4
PBAT(20)-500-2	0.020 ± 0.002	1.488	29.2
PBAT(20)-500-3	0.021 ± 0.003	1.423	27.9
PLA(10)-500-1	0.023 ± 0.002	0.963	18.9
PLA(10)-500-2	0.021 ± 0.003	0.864	16.9
PLA(10)-500-3	0.022 ± 0.003	0.945	18.5

B.3 Volume resistivity

All measurements were done in room temperature measured 22 ^0C. Thickness was averaged from 5 readings taken by rotating the sample on Solartron micrometer sample holder for 5 positions. Sample was mounted on the sample holder, whereas a fixed pressure was applied from the micrometer unit. A 100V DC voltage was applied to Solartron 30mm ring electrode assembly where the sample was mounted. Resistance at the 60th second was recorded for volume resistivity calculations.

Table B.3. *Resistance measured at 60th second, average thickness of measured samples and volume resistivity of each sample.*

Sample name	**Thickness**	**Resistance**	**Volume resistivity**
	mm	**Ω**	**Ωm**
PHB(15)-750-1	0.025 ± 0.003	9.20×10^{12}	2.71×10^{15}
PHB(15)-750-2	0.024 ± 0.003	1.09×10^{13}	3.30×10^{15}
PHB(15)-750-3	0.025 ± 0.003	1.75×10^{13}	5.07×10^{15}
PHB(15)-750-4	0.024 ± 0.002	1.09×10^{13}	3.30×10^{15}
PHB/PHV[88:12](20)-500-1	0.021 ± 0.001	1.99×10^{12}	6.86×10^{14}
PHB/PHV[88:12](20)-500-2	0.023 ± 0.003	4.22×10^{11}	1.35×10^{14}
PHB/PHV[88:12](20)-500-3	0.021 ± 0.002	3.34×10^{11}	1.15×10^{14}
PHB/PHV[88:12](20)-500-4	0.023 ± 0.003	3.61×10^{11}	1.16×10^{14}
PCL(12)-500-1	0.026 ± 0.003	4.98×10^{10}	1.38×10^{13}
PCL(12)-500-2	0.025 ± 0.003	1.34×10^{10}	3.85×10^{12}
PCL(12)-500-3	0.026 ± 0.002	1.40×10^{10}	3.88×10^{12}
PCL(12)-500-4	0.026 ± 0.003	7.38×10^{9}	2.07×10^{12}
PBS(20)-500-1	0.023 ± 0.002	1.33×10^{11}	4.24×10^{13}
PBS(20)-500-2	0.023 ± 0.002	1.78×10^{11}	5.54×10^{13}
PBS(20)-500-3	0.022 ± 0.002	2.89×10^{11}	9.61×10^{13}
PBS(20)-500-4	0.023 ± 0.003	2.13×10^{11}	6.89×10^{13}
PBAT(20)-500-1	0.022 ± 0.003	1.02×10^{11}	3.35×10^{13}
PBAT(20)-500-2	0.020 ± 0.002	1.49×10^{11}	5.33×10^{13}
PBAT(20)-500-3	0.021 ± 0.003	1.45×10^{11}	5.00×10^{13}

Continued on next page

Table B.3 – *Continued from previous page*

Sample name	**Thickness**	**Resistance**	**Volume resistivity**
PBAT(20)-500-4	0.020 ± 0.002	1.56×10^{11}	5.83×10^{13}
PBAT(20)-500-5	0.020 ± 0.001	1.73×10^{11}	6.25×10^{13}
PLA(10)-500-1	0.023 ± 0.002	5.69×10^{11}	1.84×10^{14}
PLA(10)-500-2	0.021 ± 0.003	4.54×10^{11}	1.58×10^{14}
PLA(10)-500-3	0.022 ± 0.003	5.19×10^{11}	1.74×10^{14}
PLA(10)-500-4	0.021 ± 0.002	5.92×10^{11}	2.02×10^{14}